PUCRS

ESCOLA DE CIENCIAS DA SAUDE E DA VIDA
PROGRAMA DE PÓS-GRADUAÇÃO EM ECOLOGIA E EVOLUÇÃO DA BIODIVERSIDADE
DISSERTAÇÃO DE MESTRADO ZOOLOGIA

PAULA TUPINAMBÁ KUSIAK FERNANDES

INTEGRATIVE TAXONOMY OF *OSTEOCEPHALUS PLANICEPS* (ANURA: HYLIDAE): new insights into its phenotypic and genetic variation and their implications for systematics

Porto Alegre
2022

PÓS-GRADUAÇÃO - *STRICTO SENSU*

Pontifícia Universidade Católica
do Rio Grande do Sul

PONTIFÍCIA UNIVERSIDADE CATÓLICA DO RIO GRANDE DO SUL

ESCOLA DE CIÊNCIAS DA SAÚDE E DA VIDA

PROGRAMA DE PÓS-GRADUAÇÃO EM ECOLOGIA E EVOLUÇÃO DA BIODIVERSIDADE

Integrative taxonomy of *Osteocephalus planiceps* (Anura: Hylidae): new insights into its phenotypic and genetic variation and their implications for systematics

PAULA TUPINAMBÁ KUSIAK FERNANDES

DISSERTAÇÃO DE MESTRADO

PONTIFÍCIA UNIVERSIDADE CATÓLICA DO RIO GRANDE DO SUL

Av. Ipiranga 6681- Caixa Postal 1429

Fone: (051) 3320-3500

CEP 90619-900 Porto Alegre – RS- Brasil

2022

PONTIFÍCIA UNIVERSIDADE CATÓLICA DO RIO GRANDE DO SUL

ESCOLA DE CIÊNCIAS DA SAÚDE E DA VIDA

PROGRAMA DE PÓS-GRADUAÇÃO EM ECOLOGIA E EVOLUÇÃO DA BIODIVERSIDADE

Integrative taxonomy of *Osteocephalus planiceps* (Anura: Hylidae): new insights into its phenotypic and genetic variation and their implications for systematics

Dissertação apresentada como requisito para a obtenção do grau de Mestre pelo Programa de Pós-Graduação em Ecologia e Evolução da Biodiversidade da Escola de Ciências da Saúde e da Vida da Pontifícia Universidade Católica do Rio Grande do Sul.

Paula Tupinambá Kusiak Fernandes

Orientador: Dr. Marco Brandalise

Co-orientador: Dr. Santiago Castroviejo-Fisher

DISSERTAÇÃO DE MESTRADO

Porto Alegre – RS – Brasil

2022

SUMÁRIO

AGRADECIMENTOS

Primeiramente, aos meus orientadores Marco Brandalise e Santiago Castroviejo-Fisher pela confiança em me guiar nessa etapa da minha vida. Em especial ao Santi por ter me acolhido como aprendiz de herpetologia desde a graduação, o que foi extremamente decisivo para eu me apaixonar por sapos e querer seguir uma vida acadêmica estudando esses animais incríveis. Agradeço ao Marco por ter me cedido uma vaga em seu laboratório para que eu pudesse entrar no programa de Pós-graduação da PUCRS.

Aos meus colegas de laboratório Andrés, Lourdes, Moisés, Victor e Omar por sempre estarem dispostos a me ajudarem e me acolherem com carinho. Sem os ensinamentos de vocês esse momento da minha vida teria sido bem mais estressante.

Aos meus amigos Dr. Giussepe Gagliardi e Omar Rojas que me acolheram na minha primeira experiência de campo na Amazônia. Giussepe, você me acolheu na sua casa, me tratou como uma irmã mais nova, me ensinou tudo sobre como fazer trabalho de campo, como lidar com uma nova cultura e como achar animais em uma floresta, esses meses que passei com você foram essenciais na minha vida. Omar, teu companheirismo e experencia foram fundamentais para que a nossa expedição pudesse ser concluída com sucesso.

À minha amiga Maria Eduarda que embarcou comigo nessa experiencia de vida, que foi a expedição para Amazônia. Com tua amizade e presença tudo se tornou mais leve. Me ajudou em momentos de ansiedade, momentos de medo das aranhas e com ensinamentos culinários. Fico muito feliz do que passamos juntas e não vejo a hora de fazermos outra viagem.

Aos meus amigos de fora da vida acadêmica, em especial Victoria, Luísa, Isabella, Marina, Vitor, Debora e Naiama que em momentos de lazer puderam me abstrair dos momentos de ansiedade da dissertação. A leveza de estar com vocês foi

essencial para que eu conseguisse passar por esse momento sem absorver o estresse de um mestrado.

À CAPES, pela bolsa concedida.

E por último e nada menos importante aos meus pais, Aline e Paulo. Por todo esforço, carinho, amor, paciência e investimento depositado em mim desde que eu nasci. O apoio de vocês sempre foi a maior base da minha vida, desde quando eu era criança vocês sempre me botaram em contato direto com a natureza, sempre me levaram para trilhas, acampamentos e banhos de rios, tenho certeza de que não foi por acaso que quis seguir o caminho da biologia, sempre foram vocês. Vocês sempre me acolheram, sem nenhum julgamento de escolhas na minha vida, não maneira de conseguir retribuir vocês por tudo que fizeram por mim, amo muito vocês.

RESUMO

A Bacia Amazônica ocidental abriga o maior número de espécies de anfíbios por área no mundo. Apesar do incremento dos estudos filogenéticos e das descrições de espécies novas, ainda há grandes lacunas de conhecimento nas espécies descritas. Isto gera incerteza taxonômica e dificulta o avanço do conhecimento sobre a biodiversidade e sua conservação. Essas lacunas estão particularmente associadas com espécies descritas no século XIX baseadas em um ou poucos espécimes, frequentemente mal preservados e com ambiguidade na designação do material e/ou a localidade tipo. Este é o caso da perereca *Osteocephalus planiceps* (Hylidae), superficialmente descritas com base em um espécime em 1874 por Cope. O que se conhece sobre *O. planiceps* é resumida a breve caracterização feita 171 anos depois de sua descoberta e informações adicionais indiretas de estudos focados na descrição de novas espécies. Porém, na maioria dos espécimes usados para realizar as comparações morfológicas nos estudos, são espécimes equatorianos e sem relatos de espécimes topotípicos desde a descrição original. Ou seja, atualmente não se tem precisão sobre os caracteres e variações fenotípicas de espécimes de *O. planiceps*, o que também levanta dúvidas sobre nosso conhecimento sobre sua distribuição. Considerando esse contexto, fizemos buscas ativas em campo em três localidades em Loreto, Peru: Estación Biológica José Álvarez Alonso (EBJAA), Centro de Investigación Jenaro Hererra – José Lopez Parodi (CIJH) e Comunidade Frontera. Estudamos variação genotípica e fenotípica, incluindo morfologia externa, morfometria, osteologia e sequências de DNA de *O. planiceps*. Coletamos 50 espécimes (19 machos, 26 fêmeas e 5 juvenis) em adicional, estudamos 53 espécimes de *Osteocephalus* das coleções do Museu de Ciências e Tecnologia da PUCRS e do Instituto Nacional de Pesquisas da Amazônia. Medimos 16 variáveis morfométricas de 49 indivíduos. Extraímos DNA e sequenciamos dois fragmentos dos genes mitocondriais 16S (~590 bp) e COI (~610 bp) de 29 indivíduos de diferentes localidades. Estudamos a osteologia de 9 espécimes usando *microCT-scan* e modelos 3D com o *software* Avizo. Pelo fato de *O. planiceps* e *O. vilarsi* serem espécies congenéricas, incluímos espécimes de *O. vilarsi* nas análises de morfologia externa, morfometria, filogenia e osteologia a fim de fazer comparações entre as espécies. Nossos resultados revelam: (i) variação genética previamente desconhecida e estrutura hierárquica dentro de *O. planiceps* e *O. vilarsi*; (ii) relação filogenética irmã entre as espécies citadas; (iii) primeira descrição osteológica detalhada e completa para ambas as espécies; (iv) variação fenotípica previamente desconhecida para ambas as espécies, incluindo a descoberta de polimorfismo intraespecífico da cor óssea em *O. planiceps*, e sobreposição de todos os caracteres diagnósticos previamente sugeridos; (v) novos dados sobre a distribuição e história natural de *O. planiceps*, incluindo reidentificação de populações erroneamente atribuídas a *O. planiceps* e seu primeiro registro confirmado para o Brasil; (vi) a proposta de quatro novos caracteres osteológicos diagnósticos entre *O. planiceps* e *O. vilarsi*; e (vii) novos insights sobre a diversidade e distribuição de espécies do grupo de espécies *O. leprieurii* derivados da análise filogenética de sequências de DNA. À luz de nossos resultados, discutimos o status taxonômico de *O. vilarsi* em relação a *O. planiceps*, a relevância de alguns caracteres fenotípicos (ou seja, coloração óssea, cristas frontoparietais e um processo recém-descoberto do coracóide) na sistemática de *Osteocephalus*, e a diversidade de espécies dentro do grupo de espécies de *O. leprieurii*.

Palavras-chave: Amazonia; coloração de ossos; delimitação de espécies; morfologia; osteologia; filogenética; perereca.

ABSTRACT

The western Amazon Basin harbors the largest number of amphibian species by area in the world. Despite the increase in phylogenetic studies and descriptions of new species, there are still large gaps in knowledge of the described species. This creates taxonomic uncertainty and difficult progress of biodiversity knowledge and conservation. These gaps are frequently associated with species described in the 19th century based on one or a few specimens, often poorly preserved, and with ambiguity in material designation and/or type locality. This is the case of the treefrog *Osteocephalus planiceps* (Hylidae), briefly described from a single specimen in 1874 by Cope. What we currently known about *O. planiceps* derives from a 171 years old cursory characterization of its external morphology and additional indirect information from studies focusing on the description of new species, with no reports of topotypical specimens since the original description. Considering this context, we performed expeditions to three localities in Loreto, Peru: Estación Biológica José Álvarez Alonso (EBJAA), Centro de Investigación Jenaro Hererra – José Lopez Parodi (CIJH), and Comunidad Frontera. We studied genotypic and phenotypic variation, including external morphology, morphometry, osteology and DNA sequences of *O. planiceps*. We collected 50 specimens (19 males, 26 females and 5 juveniles) in addition, we studied 53 specimens of *Osteocephalus* from the collections of the Museu de Ciências e Tecnologia da PUCRS and Instituto Nacional de Pesquisas da Amazônia. We measured 16 morphometric variables from 49 individuals. We extracted DNA and sequenced two fragments of mitochondrial genes 16S (~590 bp) and COI (~610 bp) from 29 individuals from different locations. We studied the osteology of 9 specimens using microCT-scan and 3D models. Because *O. planiceps* and *O. vilarsi* are the most similar congeneric species, we included detailed comparisons of the two species for all sets of characters. Our results reveal: (i) previously unknown genetic variation and hierarchical structure within both *O. planiceps* and *O. vilarsi*; (ii) sister phylogenetic relationship between the aforementioned species; (iii) first detailed and complete osteological description for both species; (iv) previously unknown phenotypic variation for both species, including the discovery intraspecific polymorphism of bone color in *O. planiceps*, and overlap of all previously suggested diagnostic characters; (v) new data on the distribution and natural history of *O. planiceps*, including reidentification of populations wrongly assigned to *O. planiceps* and its first confirmed record for Brazil; (vi) the proposal of four new diagnostic osteological characters between *O. planiceps* and *O. vilarsi*; and (vii) new insights into the species diversity and distribution of the *O. leprieurii* species group derived from phylogenetic analysis of DNA sequences. In light of our results, we discuss the taxonomic status of *O. vilarsi* in relation with *O. planiceps*, the relevance of some phenotypic characters (i.*e*., bone coloration, frontoparietal ridges, and a newly discovered process of the coracoid) in *Osteocephalus* systematics, and the species diversity within *O. leprieurii* species group

Keywords: Amazonia; bone coloration; species delimitation; morphology; osteology;

phylogenetics; tree frogs.

1. INTRODUÇÃO GERAL

Osteocephalus Steindachner, 1862 é um grupo monofilético de pererecas arbóreas, noturnas, de tamanho médio a grande (comprimento rostro-cloaca SVL= 31.0–109.8 mm), com uma ampla distribuição na América do Sul, desde Colômbia até a Bolívia, no leste até as áreas costeiras da Venezuela e das Guianas, o centro-oeste (Mato Grosso e Mato Grosso do Sul) e nordeste do Brasil (Piauí) (Jungfer *et al*. 2013; Carvalho *et al*. 2017). Mesmo que a maioria das espécies do gênero sejam restritas às terras baixas, algumas podem chegar até 2000 m s.n.m (Jungfer 2015).

Atualmente são reconhecidas 27 espécies de *Osteocephalus* (Frost 2022) organizadas em cinco grupos monofiléticos de espécies (sensu Jungfer et al. 2013): *O. alboguttatus*, *O. buckleyi*, *O. leprieurii*, *O. planiceps* e *O. taurinus*. As únicas sinapomorfias fenotípicas do gênero são indivíduos recém metamorfoseados com íris vermelha e marcas claras nos membros (Jungfer *et al*. 2013), o que limita a capacidade de identificação de adultos e girinos. Características comuns de adultos de *Osteocephalus*, porém variáveis no gênero, são: crânio fortemente ossificado, com cristas frontoparietais lateralmente elevadas e visíveis (Trueb & Duellman 1970); e íris dourada entremeada por linhas escuras brilhantes (Jungfer 2015). Além disso, parte das espécies desse gênero apresentam dimorfismo sexual: machos apresentam tubérculos ou até mesmo espinhos na parte dorsal da pele; fêmeas apresentam o dorso mais ou menos liso, sem tubérculos ou espinhos (Jungfer *et al*. 2013).

Os *Osteocephalus* sempre apresentaram problemas de taxonomia, filogenia e identificação. Jungfer *et al*. (2013) apresentou um estudo sobre a complexidade da filogenia do gênero, retirando espécies antes identificadas como *Osteocephalus* e reagrupando em outros gêneros como *O. aecii* Señaris, and Gorzula, 1993, transferida. Além disso outras espécies foram postas como sinonímia, como é o caso de

Osteocephalus vilmae Ron, Venegas, Toral, Read, Ortiz & Manzano, 2012 é colocado na sinonímia de *O. buckleyi* Boulenger, 1882. Outra resolução importante vinda deste trabalho foi a definição dos cinco grupos espécies mencionadas anteriormente.

Apesar do incremento dos estudos filogenéticos e das descrições de espécies novas (Duellman, 2019; Ferrão *et al*. 2019; Blotto *et al*. 2020; Chasiluisa, Caminer, Varela-Jaramillo, and Ron, 2020; Melo-Sampaio, Ferrão, and Moraes, 2021), ainda há grandes lacunas de conhecimento nas espécies descritas. Isto gera incerteza taxonômica e dificulta o avanço do conhecimento sobre a biodiversidade e sua conservação. Essas lacunas estão particularmente associadas com espécies descritas no século XIX baseadas em um ou poucos espécimes, frequentemente mal preservados e com ambiguidade na designação do material e/ou a localidade tipo. Como é o caso de *Osteocephalus planiceps*, uma espécie do gênero descrita em 1874 por Cope.

Osteocephalus planiceps foi descrita baseada em um único macho, coletado em Nauta, departamento de Loreto, Peru, sua descrição é breve sem apresentar detalhes sobre variação da espécie. Além disso *O. planiceps* foi proposto como sinonímia júnior de *O. taurinus* Steindachner, 1862, devido às suas semelhanças no tamanho do corpo e à presença de bordas laterais nitidamente elevadas dos frontoparietais (Trueb & Duellman 1971). Após uma investigação mais aprimorada no holótipo e mais alguns indivíduos recém coletados de *O. planiceps*, Duellman & Mendelson (1995) revalidaram como espécie. Outras informações sobre *O. planiceps* apareceram ao longo dos anos, como na descrição de *O. yasuni* (Ron & Pramuk 1999) que foi incluso uma breve descrição osteológica do crânio das duas espécies. Este estudo também representa a primeira menção à coloração dos ossos de *O. planiceps*. A sua distribuição já era conhecida no Peru e no Ecuador (Ron & Pramuk 1999), então Gordo & Neckel-Oliveira (2004) e Lynch (2008) discutiram a distribuição no Brasil e na Colômbia, respectivamente.

Jungfer (2010) revalidou *O. vilarsi* (Melin, 1941) observando sua alta similaridade com *O. planiceps* e sugeriu que os registros brasileiros desta última espécie podem representar *O. vilarsi*. Ferrão *et al*. (2019) realizou um estudo na região do alto Rio Negro, incluindo espécimes de *O. planiceps* e espécies candidatas Escudo das Guianas Ocidental (Jungfer *et al*. 2013) concluindo que eles fazem parte de *O. vilarsi*. Como caracteres diagnósticos que suportam a diferenciação entre *O. planiceps* e *O. vilarsi*, Ferrão *et al*. (2019) listaram diferenças na cor dos ossos tibiofibulares em vida, cor da íris em metamorfos, espaço morfométrico não sobreposto entre fêmeas adultas na análise de PCA e duração do canto dos cantos de anúncio.

O que se conhece sobre *O. planiceps* é resumida a breve caracterização feita por Duellman & Mendelson (1995) e informações adicionais indiretas de estudos focados na descrição de novas espécies (Ron & Pramuk 1999; Jungfer *et. al*. 2000; Jungfer & Lehr 2001; Jungfer & Hold 2002; Moravec *et al*. 2009; Jungfer 2010; Ron *et al*. 2010; Ferrão *et al*. 2019). Porém, na maioria dos espécimes usados para realizar as comparações morfológicas nos estudos citados acima, são espécimes equatorianos e sem relatos de espécimes topotípicos desde a descrição original. Ou seja, atualmente não se tem precisão sobre os caracteres e variações fenotípicas de espécimes de *O. planiceps*, o que também levanta dúvidas sobre nosso conhecimento sobre sua distribuição.

CAPÍTULO 1

Tupinambá, P. (2022). Integrative taxonomy of *Osteocephalus planiceps* (Anura: Hylidae): new insights into its phenotypic and genetic variation and their implications for systematics.

Manuscrito formatado para artigo

O trabalho será submetido para a revista *Zootaxa* em co-autoria com (ordem alfabética): Andres Felipe Jaramillo-Martinez, Fernando J. M. Rojas-Runjaic, Giussepe Gagliardi-Urrutia, Karl-Heinz Jungfer, Pedro Ivo Simões e Santiago Castroviejo-Fisher. O manuscrito está formatado segundo as normas da revista citada acima.

Integrative taxonomy of *Osteocephalus planiceps* (Anura: Hylidae): new insights into its phenotypic and genetic variation and their implications for systematics

Paula Tupinambá

Laboratório de Sistemática de Vertebrados, Pontifícia Universidade Católica do Rio Grande do Sul, Porto Alegre 90619-900, Rio Grande do Sul, Brasil. Tel: +55 51 3320-4411 e-mail: paulatupikf@gmail.com

Abstract

What we currently known about *Osteocephalus planiceps* derives from a 171 years old cursory characterization of the external morphology of a single specimen and additional indirect information from studies focusing on the description of new species, with no reports of topotypical specimens since the original description. Considering this context, we performed expeditions to three localities in Loreto, Peru, and collected fresh specimens (26 females, 19 males, and 5 juveniles), including tissue samples and associated data. We studied genotypic and phenotypic variation, including external morphology, morphometry, osteology and DNA sequences of these material and from 53 additional specimens of *Osteocephalus* from scientific collections. We measured 16 morphometric variables from 49 individuals. We extracted DNA and sequenced two fragments of mitochondrial genes 16S (~590 bp) and COI (~610 bp) from 29 individuals from different locations. We studied the osteology of 9 specimens using microCT-scan and 3D models. Because *O. planiceps* and *O. vilarsi* are the most similar congeneric species, we included detailed comparisons of the two species for all sets of characters. Our results reveal: (i) previously unknown genetic variation and hierarchical structure within both *O. planiceps* and *O. vilarsi*; (ii) sister phylogenetic relationship between the aforementioned species; (iii) first detailed and complete osteological description for both species; (iv) previously unknown phenotypic variation for both species, including the discovery intraspecific polymorphism of bone color in *O. planiceps*, and overlap of all previously suggested diagnostic characters; (v) new data on the distribution and natural history of *O. planiceps*, including reidentification of populations wrongly assigned to *O. planiceps* and its first confirmed record for Brazil; (vi) the proposal of four new diagnostic osteological characters between *O. planiceps* and *O. vilarsi*; and (vii) new insights into the species diversity and distribution of the *O. leprieurii* species group derived from

phylogenetic analysis of DNA sequences. In light of our results, we discuss the taxonomic status of *O. vilarsi* in relation with *O. planiceps*, the relevance of some phenotypic characters (i.*e*., bone coloration, frontoparietal ridges, and a newly discovered process of the coracoid) in *Osteocephalus* systematics, and the species diversity within *O. leprieurii* species group.

Keywords: Amazonia; bone coloration; species delimitation; morphology; osteology; phylogenetics; tree frogs.

Introduction

Osteocephalus Steindachner, 1862 is a monophyletic group of medium to large-sized (snout–vent length, SVL, = 31.0–109.8 mm) arboreal frogs (Jungfer *et al*. 2013). It has a wide distribution across the northern half of South America east of the Andes. Besides Amazonia, the Andes, and the Guianas, there are records in the central-west (Mato Grosso and Mato Grosso do Sul) and northeast (Piauí) of Brazil (Jungfer *et al*. 2013; Carvalho *et al*. 2017). Even though most species of the genus are restricted to the lowlands, some reach up to 2000 m a.s.l. (Jungfer 2015).

The current understanding of the phylogenetic relationships among *Osteocephalus* species and their placement within Hylidae are rather uncontroversial (Jungfer *et al*. 2013; Blotto *et al*. 2020). All studies agree that *Osteocephalus* is nested within Lophyohylini and more closely related with the genera *Dryaderces*, *Osteopilus*, and *Tepuihyla* (see summary in Blotto *et al*. 2020). Also, since Jungfer *et al*. (2013), the species of *Osteocephalus* are organized in the following monophyletic species groups, also with little disagreement: *O. alboguttatus*, *O. buckleyi*, *O. leprieurii*, *O. planiceps*, and *O. taurinus*.

The species level-systematics of the genus is clearly more at flux, with 44 % of the 27 currently recognized species described since 2000 (Frost 2022). Furthermore, several studies based of analyses of DNA sequences showed that there is a number of undescribed candidate species, indicating that the current recognized species richness is likely underestimated (Moravec *et al*. 2009; Ron *et al.* 2010, 2012; Jungfer *et al*. 2013; Blotto *et al.* 2020; Chailuisa *et al*. 2020). Besides the discovery of new species through the exploration of poorly sampled geographic areas and the application of new technologies and analytical tools (*e.g.*, Duellman 2019; Melo-Sampaio *et al*. 2021), species delimitation within some *Osteocephalus* taxa is particularly challenging. These

taxa are responsible for several controversial cases of species splits and lumps. The most recalcitrant ones involve widely distributed species expanding over important geographic barriers, such as large Amazonian rivers, and named in the XIX century through a cursory description of the external morphology of one or very few preserved specimens. Examples are *O. buckleyi* (Boulenger, 1882), *O. leprieurii* (Duméril and Bibron, 1841), *O. planiceps* Cope, 1874, and *O. taurinus* Steindachner, 1862. These taxa show remarkable phenotypic variation in characters commonly used to diagnose species of *Osteocephalus* and the divergence among DNA sequences of specimens from different localities and from the most closely related species is very low or even overlap, often resulting in poorly resolved phylogenetic relationships and short branches (Jungfer & Hold 2002; Jungfer 2010; Jungfer *et al*. 2013; Ferrão et al. 2019).

The original description of *Osteocephalus planiceps* was based on a single male (SVL = 58.5 mm; Fig. 1) collected from Nauta, department of Loreto, Peru (Cope 1874; Malnate 1971). The description is accurate but brief—following the standards of its time—and only allows meaningful comparisons with two other species (*O. leprieuri* and *O. taurinus*) since it was the third described species of the genus. Nothing of substance was published about *O. planiceps* until it was proposed as a junior synonymy of *O. taurinus* due to their similarities in body size and the presence of distinctly elevated lateral edges of the frontoparietals (Trueb & Duellman 1971). Duellman & Mendelson (1995) revalidated *O. planiceps* after studying the holotype and over a dozen freshly collected specimens from Loreto, between the Pastaza and Tigre rivers, Peru, on the border with Ecuador. This study provided much needed information on variation, including sexual dimorphism, and coloration in life. However, the redescription focused on its diagnosis with *O. taurinus* and lacked fresh material from the type locality, so that

the information included would prove limited for future research as more than a dozen species have been described afterwards.

When Ron & Pramuk (1999) described *O. yasuni*, they also included a description and illustration of both the cranial osteology—based on a single specimen from Ecuador—and the advertisement call—based on a recording from a specimen from Loreto, Peru—of *O. planiceps*. This study also represents the first mention to the coloration of bones of *O. planiceps*, which are described as green in life and used as a diagnostic character. Gordo & Neckel-Oliveira (2004) and Lynch (2008) discussed the distribution of *O. planiceps* in Brazil and Colombia, respectively. Moravec *et al.* (2009) described *O. castaneicola*, a morphologically similar and closely related species to *O. planiceps* from northern Bolivia and southern Peru. Jungfer (2010) revalidated *O. vilarsi* (Melin, 1941) noting its high similarity with *O. planiceps* and suggested that the Brazilian records of the latter species by may represent *O. vilarsi*. Jungfer *et al*. (2013) presented the first densely sampled quantitative phylogenetic study of *Osteocephalus* and established the *O. planiceps* species group including: *O. castaneicola*, *O. deridens*, *O. fuscifacies*, *O. leoniae*, *O. planiceps*, and a undescribed new species most similar to *O. planiceps* from the western Guiana Shield. Finally, Ferrão *et al*. (2019) studied a large series of *Osteocephalus* from the upper Rio Negro region (including the only reported Brazilian specimens of *O. planiceps* and the aforementioned candidate species from the western Guiana Shield similar to *O. planiceps*) concluding that they are part of *O. vilarsi*. Accordingly, they expanded the description of *O. vilarsi*, which was previously only known from the holotype, noting that the most similar species of the genus in external morphology and bioacoustics is *O. planiceps*. However, they were not recovered as sister species in phylogenetic analyses (Jungfer *et al.* 2013; Ferrão *et al*. 2019; Blotto *et al*. 2020). As diagnostic characters supporting the differentiation

between *O. planiceps* and *O. vilarsi*, Ferrão *et al*. (2019) listed differences in color of tibiofibular and femur bones in life, color of iris in metamorphs, non-overlapping morphometric space among adult females in PCA analysis, and call duration of advertisement calls.

Since Duellman & Mendelson (1995) brief characterization, all information about the phenotypic variation within *O. planiceps* is indirect as it derives from studies focusing on the description of new species similar to it or on larger evolutionary issues (Ron & Pramuk 1999; Jungfer *et al.* 2000; Jungfer & Lehr 2001; Jungfer & Hold 2002; Moravec *et al.* 2009; Jungfer 2010; Ron *et al.* 2010; Jungfer *et al.* 2013; Ferrão *et al*. 2019; Blotto *et al*. 2020; Moura *et al*. 2021). Furthermore, most information derives from Ecuadorian specimens without reports of topotypic specimens since the original description (Cope 1874) or on series of Peruvian specimens most likely including specimens of *O. castaneicola* (*e.g.*, Jungfer 2010). In a nutshell, it is currently unclear how to phenotypically characterize and identify specimens of *O. planiceps*, which also cast doubts about our knowledge of its distribution and the identification of specimens used in molecular phylogenetics, and the available information is not only scarce but sparse across many studies. Considering this context, we collected new material from near the type locality and studied their genotypic and phenotypic variation including external morphology, morphometrics, osteology, and DNA sequences. This allowed us to identify as *O. planiceps* specimens from other localities with greater confidence and subsequently incorporate previously unknown variation. Our results challenge some conclusions of previous studies based on smaller sampling, which we discuss in detail.

Materials and Methods

Field work. We performed expeditions to three different localities of the Peruvian Amazonia in 2017 (January, March, April, May, and June), 2018 (February, March,

April, and May) and 2021 (January and February) (Fig. 2). These localities are: Estación Biológica José Álvarez Alonso (EBJAA hereafter) in Maynas, Loreto, 23 km southwest of the city of Iquitos (03.964699º S, 73.418547º W), and about 75 km of uninterrupted terra-firme forest from Nauta, the type locality of *O. planiceps*; Centro de Investigación Jenaro Herrera - José Lopez Parodi (CIJH hereafter) in the district of Jenaro Herrera, Requena, Loreto, 200 km south of Iquitos (04.89923º S, 73.65062º W); and Comunidad Nativa Frontera (Frontera hereafter), located on the edges of the Rio Blanco, 310 km south of Iquitos (05.879362º S, 73.76045º W). We photographed in life all collected specimens, which were later euthanized with an overdose of topical 5 % lidocaine solution. We removed from every specimen a piece of muscle from the hind limb and/or liver and preserved it in 96 % ethanol for molecular analyses. We fixed all specimen in 10 % formalin solution for two days and preserved them in 70 % ethanol. We deposited all collected specimens in the amphibian collections of Museu de Ciências e Tecnologia of the Pontifícia Universidade Católica do Rio Grande do Sul (MCP) and Colección Referencial de Biodiversidade del Instituto de Investigaciones de la Amazonia Peruana (CRBIIAP). We list voucher codes and additional relevant information in Appendix 1.

External morphology. In addition to the specimens that we collected in the aforementioned expeditions, we also examined alcohol-preserved specimens housed at MCP, CRBIIAP, and the Herpetological section of the Zoological Collection of Instituto Nacional de Pesquisas da Amazônia (INPA-H). We list studied specimens and their associated information in Appendix 1. The format for species characterization and description is updated from Duellman (1970). Webbing formula is that of Savage and Heyer (1967), as modified by Myers and Duellman (1982). Terminology of limb folds follows Kok & Castroviejo-Fisher (2008). We determined sex and maturity by body

size and presence of secondary sexual characters (*e.g*., vocal sac, vocal slits, skin texture, nuptial excrescences on prepollex, presence of eggs). Using a digital caliper or a stereo microscope with a graduated lens (precision 0.1 mm), we measured the following 16 morphometric variables: snout-to-vent length, distance from tip of snout to posterior margin of vent (SVL); head length, from tip of snout to posterior edge of maxilla articulation (HL); head width, at the level of maxilla articulation (HW); eye-to-nostril distance, from anterior corner of the eye to the center of nostril (END); eye diameter, from anterior to posterior corner (ED); interorbital distance, between the anterior corners of the orbits (IOD); internarial, distance from between the inner margins of the nostrils (IND); nostril-snout distance, from tip of snout to the center of nostril (NSD); horizontal tympanum diameter (TD); vertical tympanum diameter (VTD); thigh length, distance from the outer surface of the flexed knee to the heel/tibiotarsal inflection (TL); tibia length, distance from the vent to the knee (THL); foot length, from proximal edge of inner metatarsal tubercle to tip of Toe IV (FL); fourth toe disk diameter, width of disc on Toe IV (4TD); and third finger disk diameter, width of disc on Finger III (3FD).

Morphometric analysis. Because *Osteocephalus planiceps* and *O. vilarsi* are the most similar congeneric species (Ferrão *et al*. 2019), we used a Principal Component Analyses (PCA) to explore their potential differentiation in the morpho-space and evaluate the variables with the highest loadings. We restrict our analysis to adult specimens and labelled males and females differently to detect sexual dimorphism. We performed two PCAs: one with the raw measurements and other removing the effect of size by using the residuals of a linear regression of each morphological variable against SVL. We performed PCAs using the function 'prcomp()' of the stats package of R. To test for statistical significance between overlapping variables, we performed a non-parametric pairwise Wilcoxon test (data violated the normality and homogeneity

assumptions of parametric tests) using the function 'pairwise.wilcox.test()' of the stats package in R.

Osteology. We scanned four *O. planiceps* (MCP 14001, MCP 14012, MCP 14490 and 14492) and five *O. vilarsi* (MCP 13447, MCP 13449, MCP 13450, INPAH 40470, and INPAH 40468) on a SkyScan 1173 Micro-CT scanner at the Instituto do Petróleo e dos Recursos Naturais (IPR-PUCRS), see Appendix 1 for specimen data. We set tube voltage and current at 60 kV and 75 μA, respectively, and voxel resolution was 25 μm. We visualized 3D models and created images for figures using Avizo 2019.1 (Bruker MicroCT). Cranial terminology follows Trueb (2015) and postcranial terminology follows Duellman and Trueb (1986) and Trueb (1973), manus and pes follow Fabrezi (1992, 1993, 2001), and ilium follows Gómez and Turazzini (2016).

Molecular laboratory protocols. We extracted genomic DNA from 29 preserved tissue samples of *O. planiceps*, *O. vilarsi*, *O. leprieurii*, *O. yasuni*, *O. castaneicola*, and *O. taurinus* using the Wizard Genomic DNA Purification Kit (Promega, Madison-WI, USA) following the manufacturer's instructions. We used the polymerase chain reaction (PCR) for each sample for a total volume of 25.0 μL, containing 2.0 μL of genomic DNA, 12.5 μL (1X) of Hot Star Taq Master Mix-Qiagen, 0.75 μL (0.3 μM) for each primer, 0.75 μL (1.5 mM) of $MgCl_2$ and 8.25 μL with MiliQ H2O to complete the total volume. We amplified a fragment of two mitochondrial genes, 16S (~ 590 bp) and cytochrome oxidase I (COI, ~ 610 bp). For 16S, we used the universal primers 16Sar (5′- CGCCTGTTTATCAAAAACAT -3′) and 16Sbr (5′- CCGGTCTGAACTCAGATCACGT -3′) (Palumbi 1991), with the following PCR conditions: initial denaturation 95°C – 15 min, followed by 35 cycles of 94°C – 0.5 min, 50°C – 0.5 min and 64°C – 1 min, and final extension 72°C – 10 min. For COI, we used the primers T3- AnF1 (5′-

ATTAACCCTCACTAAAGACHAAYCAYAAAGAYATYGG -3′) and T7- AnR1 (5′-AATACGACTCACTATAGCCRAARAATCARAADARRTGTTG -3′) of Lyra *et al*. (2017), with the following PCR conditions: The initial activation at 95 °C – 20 min, followed by two groups of cycles, the first where performed using 10 cycles at 94 °C – 0.5 min, 45 °C – 0.5 min with an increase of 0.5 °C in each cycle and 64°C – 1 min, the second group of 25 cycles where used to enrich the initial products at 94 °C – 0.5 min, 50 ° C – 0.5 min and 64 °C – 1 min, final extension at 72 °C – 10 min and polymerase inactivation at 4 °C – 10 min. We sequenced PCR products in both directions using Sanger sequencing. We used Sequencher 4.1.4 (Gene Codes Corporation, Ann Arbor, MI, USA) to assemble contigs and edit the consensus sequence by direct inspection of the original chromatographs.

Phylogenetic analyses. We downloaded from GenBank homologous sequences of representatives of 68 *Osteocephalus* nominal species, which represent all currently recognized species with data in GenBank. We also used GenBank sequences from *Dryaderces pearsoni* and *Tepuihyla rodriguezi* as outgroups and from *Phyllodytes brevirostris* as the root. To complement the two mitochondrial markers that we sequenced, we also downloaded DNA sequences of the following genes according to the dataset of Blotto *et al*. (2020): 12S, tRNA-Val, 16S, ND1, COI, Cytb, POMC, RAG-1, RHOD, SIAH, TNS3, and TYR. We list in Appendix 2 all voucher specimens and their corresponding GenBank accession numbers. We individually aligned sequences of each marker using MUSCLE (Edgar, 2004) in AliView (Larsson, 2014) under default parameters. To reduce the numbers of missing entries per terminal and search space during phylogenetic analyses (Wilkinson, 1995; Kearney, 2002; Brower, 2018), in one case (*O. cabrerai*) we assigned sequences from two different specimens of the same species to a single composite terminal. We only did this with terminals of

species that are not part of the *O. planiceps* species group and when genetic distances among shared mitochondrial markers of the targeted terminals were < 1 %. We combined the alignments of the different genes into a single matrix using SequenceMatrix 1.8 (Vaidya *et al*., 2011). We divided the dataset by gene and, for protein coding genes, by codon positions. We considered indels as unknown nucleotides in all downstream analyses. We determined the most appropriate model of nucleotide substitution and data partition scheme using ModelFinder (Kalyaanamoorthy *et al*., 2017), as implemented in IQ-TREE, with the command *-m testnewmergeonly* and the Bayesian information criterion (Schwarz 1978). We performed 500 independent tree searches under the maximum likelihood (ML) criterion in IQ-TREE (Minh *et al*., 2020), with the command *-nstop* set to 500, the option *-allnni* activated, and using the models and partitions resulting from ModelFinder (Chernomor *et al*., 2016). We used default settings for other parameters. We assessed clade support with 1000 bootstrap (BS) pseudoreplicates using IQ-TREE with the same aforementioned settings. We used the SumTrees package in DendroPy v4.4.0 (Sukumaran & Holder, 2010) to add BS frequencies to the best ML tree. To assess phylogenetic resolution, we collapsed nodes incompatible with those from slightly suboptimal trees, defined as the trees from our 500 independent searches that differ from the best reported tree by < 0.1 log-likelihood unit. This value is typically an order of magnitude less than the change in log-likelihood after adding a single autapomorphy to the data matrix (Simmons & Kessenich, 2020), which for example could easily happen when introducing an error while editing chromatographs. We calculated uncorrected genetic distances from 318 bp of 16S and 646 of COI for specimens of the *O. planiceps* species group (maximum overlapping length maximizing specimen sampling).

Results

Phenotypic data. We provide detailed descriptions and comparisons of the integument and skeleton in the species account (illustrated in Figs 4–12 and 15–18, respectively), and summarize morphometric data in Table 1 and 2, and Fig. 13.

Phylogenetics. The molecular dataset includes 102 terminals, 33 of which represent described species of the *O. planiceps* species group, and 7,677 aligned positions (the dataset will be available at https://zenodo.org/). We excluded from the analyses a COI sequence from GenBank (MN953331) purportedly identified as belonging to *O. planiceps* SMNS14196 because preliminary analysis and blast searches identified it as *O. yasuni*, suggesting an identification error. The ModelFinder results selected five data partitions (Table 2). The ML optimal tree has a log likelihood score of -39153.5227 (Fig. 3) and 451 trees have < 0.1 log-likelihood unit difference (*i.e.*, we consider them as slightly suboptimal). A strict consensus of the optimal and 451 suboptimal trees show only two collapsed nodes affecting intraspecific relationships among specimens of *O. planiceps* and *O. vilarsi*, respectively (Fig. 3B). The optimal tree is well-resolved, and most clades have BS ≥ 70. Exceptions are limited to a few shallow clades involving specimens from the same species or sister species. We recover a monophyletic *Osteocephalus* as well as all its species groups except the *O. buckleyi* group. This group, as defined by Jungfer *et al*. (2013), is polyphyletic in our tree due to the position of *O. mimeticus* as the sister taxon of the clade including the remaining species of the *O. buckleyi* species group and the *O. leprieurii* species group. Other noteworthy results include the identification of specimens of *O. yasuni* from Estação Ecológica Juami-Japurá, Amazonas, Brazil, which constitute the second record of this species for the country and the northernmost locality of the species. Also, within the *O. leprieurii* species group, we recover the terminal *O*. aff. l*eprieurii* MCP 14487 from

Frontera, Loreto, Peru, as sister to all sampled specimens of *O. leprieurii* and *O. yasuni*. Genetic distances between *O*. aff. l*eprieurii* MCP 14487 and specimens of the other two species are 2.2–4.2 %, which are larger than among specimens of *O. leprieurii* and *O. yasuni*.

Within the *O. planiceps* species group, we recover *O. castaneicola* as the sister taxon of the other species of the group. Our tree shows that *O. deridens* and *O. fuscifacies* and *O. planiceps* and *O. vilarsi* are each other sister species; notwithstanding the relatively low BS values for some of the involved clades (Fig. 3B). Within *O. vilarsi*, our tree recovers two groups with 100 % BS. One includes all specimens from Juami-Japurá (MCP 13446, 13448, and 13450), while the other contains specimens from different localities across the Rio Negro basin. Genetic distances between these two groups are 0.0–2.9 % (Table 3).

Osteocephalus planiceps shows a marked hierarchical structure, although some basal groups have low bootstrap, and genetic distances are 0.0–3.4 %. However, the geographic proximity of the samples does not necessarily match the topological proximity, with several groups including specimens from distant localities and with virtually no genetic divergence or specimens from the same locality present in different groups. For example, there is a group that includes individuals from Mata da Infraero, AC, Brazil (MCP 10085), and Frontera, Peru, while another one also contains specimens from EBJAA (MCP 14492, MCP 14488, MCP 14472) mixed with those from Leticia, Colombia, and Anguilla, Loreto, Peru. It is important to note that individuals MCP 10085 and 10086 from Mata da Infraero, Cruzeiro do Sul, Acre, constitute the first confirmed report of *O. planiceps* from Brazil.

***Osteocephalus planiceps* Cope, 1874**

Trachycephalus planiceps – Knauer, 1878

Hyla planiceps – Boulenger, 1882

Osteocephalus taurinus Trueb & Duellman, 1971

Osteocephalus planiceps Duellman & Mendelson, 1995

Holotype. ANSP 11399, adult male from Nauta, departament of Loreto, Peru, collected by James Orton.

Characterization. Unless otherwise stated, descriptions refer to adult specimens. (1) SVL 48.9–67.6 mm (n = 19) in males and 50.8–80.7 mm (n = 26) in females; (2) head shape truncated and rounded in dorsal and lateral views, respectively; (3) externally evident frontoparietal ridges present in only some specimens of both sexes; (4) canthus rostralis distinct and angular, curved inwardly;(5) loreal region concave; (6) skin on dorsum of adult males with abundant and conspicuous tubercles, keratinized and bearing brown spines in breeding specimens, and scattered and smaller in females; (7) skin on flanks weakly areolate; (8) ventral skin of anterior limbs smooth and areolate on the gular region (less marked), body, and posterior limbs; (9) tympanum rounded to oval; (10) tympanic annulus distinct, (11) supratympanic fold weakly tuberculate, marked with a thin white line, extending as a rather straight line from posterior midlevel of eye to midlevel of tympanum, where it becomes sloping towards arm insertion; (12) low fringe on postaxial edge of Finger IV present, metacarpal fold formed by a row of low tubercles, ulnar fold absent but a few (1–4) low tubercles may be present in some specimens; (13) hand webbing basal between FI and II, II ($1^{3}/_{4}$–2)—(3–3^{+}) III ($2^{1}/_{2}$–$2^{3}/_{4}$)—($2^{1}/_{3}$–$2\ ^{1}/_{2}$) V; (14) oval disc of fingers large, 3FD 0.5–0.6 % (n = 19) and 0.7–0.8 % (n = 26) of TD in adult males and females, respectively; (15) subarticular tubercles on fingers large, single (except the bifid distal tubercle on finger

IV), subconical to rounded; (16) supernumerary tubercles on fingers single; (17) palmar tubercle small and round; (18) thenar tubercle large; (19) prepollex enlarged, encapsulated by skin, and not separated from the base of Finger I; (20) in life and preservative, adult males with keratinized, dark brown nuptial excrescence on the proximal side on Finger I, formed by an elevated clump of glands more concentrated on the base and extending as a thinner line to the base of the finger disc; (21) low fringe on postaxial edge of Toe V present, metatarsal fold formed by a row of low tubercles, tarsal fold and tarsal fringe absent but a few low tubercles may be present; (22) foot webbing formula I (1—1^{+})—(1–1^{+}) II (1—0^{+})—(1^{-}—1) III (1—0^{+})—($1^{1}/_{2}$—1^{-}) IV ($1^{1}/_{2}$–1^{-})—(0^{+}–1^{-}) V; (23) oval discs of toes smaller than those of fingers, 4TD 0.5 % (n = 19) and 0.6 % (n = 26) of TD in adult males and females, respectively; (24) outer metatarsal tubercle round and small; (25) inner metatarsal tubercle ovoid and protuberant; (26) subarticular tubercles on toes single and subconical; (27) supernumerary tubercles on toes single; (28) in dorsal view, a row of tubercles, each bearing a spine, on the distal side of Toes IV and V; (29) in life and preservative, dorsum of head and body grey or light to dark brown, with or without orange or reddish hues, and with very variable, in shape, size, and number, light or dark brown marks (*e.g.*, strokes, spots, blotches), most specimens have a brown intraocular blotch and white small lines bordering the darker marks, identical in preservative but orange or reddish hues become light brown; (30) in life, dorsum of limbs grey or light to dark brown, with transverse brown bands and in some specimens orange blotches, identical in preservative but orange blotches become light brown; (31) in life, flanks of body varying from cream to yellow with very variable, in size, number, and shape, brown markings (*e.g.*, strokes, spots, blotches), in preservative, flanks become grey with brown spots; (32) in life and preservative, obliquus dark brown to black band on the tympanic

region, extending anterior-posteriorly from the posterior edge of the orbit to the insertion of the arm, and delimited on the upper and lower edges by a white line; (33) in life, ventral surfaces of head, body, and limbs varying from cream to yellow, in preservative, white or cream; (34) in life and preservative, upper lip cream or white expanding into a subocular white spot usually containing small traces of brown pigmentation, lower lip brown; (35) in life and preservative, gular region with brown spots, varying in size, number, and density, that extend into the chest; (36) in life, green or white tibiofibular and femur bones, in preservative, green coloration may become white; (37) in life, iris bright golden with black reticulations irradiating from the pupil and a horizontal coper band extending from the sides of the pupil, pupillary ring absent; (38) cloaca surrounded by a circular dark brown region, which is on its upper half by a narrow pale stripe varying from hardly visible to evident; (39) males vocalize from either phytotelmata or perched on vegetation surrounding lentic water systems; (40) advertisement call of 1–4 notes lasting 108–608 ms and with a dominant frequency of 323–1162 Hz (n = 4; Ron & Pramuk, 1999; Ferrão *et al.* 2019).

Relevant variation of external morphological characters

Color in life of adults and subadults. This description is based on digital photographs of live specimens (Figs 4–7). The variation described herein does not follow a sexually dimorphic nor a life stage pattern. In other words, the patterns described herein could be present in adult or subadult females or males.

The most frequent pattern of the dorsal surfaces of head and body is a light to dark brown background with light or dark brown marks (Fig. 4A) In some specimens, the brown background color could have orange to reddish hues (*e.g.*, MCP 14480; Fig. 4B, D, E) and some specimens have a grey background coloration (Fig. 4B, G, H). The brown markings over the dorsum are irregular in shape (e.g., strokes, spots, blotches)

and very variable in size and number. For example, specimens MCP 13980 and GGU 5673 only have 4 and 3 dark small spots over the dorsum of the body, respectively, while specimens MCP 14942 and MCP 14489 have numerous brown markings of large size. Most specimens (94 %) have a transverse brown blotch between the eyes, which extends over the upper eyelids. Most specimens (62 %) have white small lines bordering the darker marks, but they are absent from some specimens such as MCP 14005. Dorsum of limbs with the same color than dorsum of body but the dark brown makings are organized as transversal bands in the former. On the forelimbs, these bands may extend from the elbow to the distal side of Finger IV, while on the hind limbs they may extend from near the cloacal region to the distal side of Toe V. At least some of the transverse bands are bordered by white lines. In some specimens (25 %), the lighter areas of the limbs are orange. On lateral view, minimally a dark brown line below the canthus rostralis extending from the nostril to the anterior edge of the orbit. This dark brown line may extend totally or partially over the canthus rostralis and the loreal region. White subocular blotch bearing traces of brown pigments that extends posteriorly—as a line below the tympanic annulus and reaching the anterior edge of the arm insertion—and anteriorly—as the white upper lip stripe. Obliquus black to dark brown band on the tympanic region, extending anterior-posteriorly from the posterior edge of the orbit to the insertion of the arm. The upper and lower edges are the tympanic annulus, and both edges are limited by a white line. Body flanks cream to yellow with very variable, in size, shape, and number, brown spots. Hidden parts of thighs light brown with hardly any markings extending in from the dorsal surfaces. Cloaca surrounded by a circular dark brown to black region limited on its upper half by a narrow white stripe varying from hardly visible to evident. Ventral surface of head, body, and limbs varying from cream to yellow. Melanophores present on all surfaces

except most of the body, where they are only present on the groin and chest. The melanophores of the gular region and chest are grouped into dots. Iris bright golden with black reticulations irradiating from the pupil and a horizontal coper band extending from the sides of the pupil, pupillary ring absent (Fig. 5). Tibiofibular bones green or white (Fig. 11). Other bones not visible through the skin.

Color in life of metamorphs and juveniles. This description is based on photographs of life specimens (Fig. 5). On recently metamorphosed specimens (Fig. 5A, B), dorsal coloration uniformly golden or dark beige, except for the elbows, knees, and ankles, which have a yellowish white patch. Iris uniformly red. More developed metamorphs are similar but show brown hues on dorsal surfaces, a reduction of the yellowish white patches on limbs, a white stripe of the upper lip, and reticulation on the iris (Fig. 5C). Juveniles are very similar to adults but the tympanic region is still similar in coloration to other surfaces (dark brown to black in adults) and the iris is weakly reticulated (markedly reticulated in adults) (Fig. 5D, E).

Color in preservative of adults and subadults. As in life but all orange and reddish areas become brown, flanks of body become greyish. The coloration of the iris becomes duller. Lower eyelid with melanophores on the upper edge, forming a line, and on the lower quarter, with other parts transparent.

Morphometrics. Table 1 summarizes the morphometric variation among adult males and females of *Osteocephalus planiceps* and *O. vilarsi*. Figure 13 illustrates the morpho-space of adult males and females of both species as inferred from PCAs. When we included the raw measurements in the PCA, the first axis explains 92.4 % of the observed variance, which corresponds with SVL, while PC2 only accounts for 1.6 % of the variance mainly corresponding with SVL, THL, and TL (Fig. 13A, Table 2). On the PCA corresponding to the residuals of a linear regression with SVL, PC1 and PC2

account for 24.9 % and 12.7 % of the variance, respectively. PC1 shows variation mainly regarding HL, HW, NSD, and THL, while in PC2 corresponds to HW, NSD, and TD. Our results clearly show that there is marked sexual dimorphism in both *O. planiceps* and *O. vilarsi*. Females tend to be larger; however, there is a great deal of overlap (Table 1, Fig. 13A, C). We find no segregation across morphometric space between specimens of the two species, with variation of specimens of *O. vilarsi* nested within that of *O. planiceps*, both when considering the raw measurements and the residuals with SVL (Fig. 13A, C). We find that when comparing the residuals with SVL, the average male HL of *O. planiceps* is larger than that of male *O. vilarsi* ($p = 0.003$), while the average female ED of *O. planiceps* is smaller than that of female *O. vilarsi* ($p = 0.002$).

Sexual and ontogenetic variation. Sexually dimorphic characters between adults include size (see previous section), dorsal skin texture, vocal sacs, and nuptial excrescences. These characters also vary between juveniles and adults. Dorsal skin texture in adult males in markedly tuberculate and visible to the naked eye. Each tubercle may bear a keratinized brown spine, but the number of tubercles with a spine and the conspicuousness of the latter structure vary among specimens, probably increasing with sexual activity. When spines are rare, they are easier to observe on the ocular and tympanic regions. Dorsal skin texture in females varies from completely smooth (*e.g.*, MCP 14005) to weakly tuberculate (*e.g.*, MCP 14942). When present, the tubercles are low (hardly or non-visible to the naked eye) and very sparse across the head, body, and limbs. Dorsal skin texture in juveniles is smooth. Males have a vocal sac that is absent in females and juveniles. The vocal sac has a complex structure; it expands medially and laterally reaching the post-tympanic fold (Moura *et al.* 2021). Males have a nuptial excrescence on the proximal side of Finger I, which is absent in

females and juveniles. It is formed by an elevated clump of glands, more concentrated on the base of the finger, and that extends, as a thin line, to the base of the finger disc. This structure is keratinized and has a conspicuous dark brown coloration. We observed a preservation artifact in which the dark brown layer is lost. In this cases, the nuptial excrescence is still evident but not its characteristic dark brown coloration.

Osteology

Considering the high similarity of *Osteocephalus planiceps* and *O. vilarsi*, their sister relationship in our phylogenetic results, and that they have not been previously described in the literature except for a few characters of the skull of a specimen of *O. planiceps* (Ron & Pramuk 1999), it is necessary to describe and illustrate the skeleton of both species. Our general characterization is based on all adult scanned specimens of both species and to avoid unnecessary repetition it applies to both taxa and sexes unless otherwise stated.

Skull

Hyperossified, with well-developed pit-and-ridge dermal sculpturing (*i.e.*, exostosis) on the frontoparietals, sphenethmoid, and nasals. It is ovoid and flat in dorsal and lateral views, respectively. Slightly wider than long. Skull length (from the margin of occipital to the tip of the snout) is 18.81–22.96 mm and 15.35–17.46 mm, and width (at the level of the quadratojugal) is 20.47–24.94 mm and 16.59–18.82 mm for *O. planiceps* and *O. vilarsi*, respectively.

Endocranium

Sphenethmoid — It is fused in a single element and forms the anterolateral wall of the neurocranium and the anterior margin of the optic foramina (Fig. 15). In dorsal view, the sphenethmoid is surrounded and contacted by the nasals and frontoparietals. It is rhombus- or pentagon-shape in *O. planiceps* and *O. vilarsi*, respectively. In ventral

view, it is flat anteriorly but concave posteriorly. It is fused with the vomers anteriorly, the neopalatines laterally, and the cultriform process of the parasphenoid posteriorly. It does not reach the otoccipital. Its margins with the cultriform process are at least distinguishable.

Otoccipital region — Composed by the completely fused exoccipitals and prootics (Fig. 15A, D). There are no clear limits among these bones, forming a single structure at the posterior part of the skull. The prootic area forms the posterolateral walls of the neurocranium and the posterior margin of the optic foramina. Dorsally, their proximal edges are fused anterolaterally with the frontoparietals, where they have a low epiotic eminence bearing on their posterior edge an elongated but short process above the condyle (Fig15A, D). The distal edge of the prootic is overlapped and fused with the proximal edge of the otic ramus of the squamosal (Fig. 15A, D). Ventrally, they are overlapped on their proximal edge by the alary process of the parasphenoid (Fig. 15B, E). The prootics are pierced by two prootic foramina. The exoccipital area forms the posteromedial wall of the neurocranium and the margins of the foramen magnum and occipital condyles. Dorsally, it is fused with the posterior edge of the frontoparietals (Fig. 15A, D). Ventrally, it is overlapped and fused by the alary and posterior processes of the parasphenoid. The shape of foramen magnum is rounded.

Middle ear — Formed by the stapes (columella) and operculum (Fig. 15B, E). The operculum is not calcified. The stapes are large, conical, with the base on the proximal side, and extending to the margins of the posterior ramus of the pterygoid.

Exocranium

Nasals — Enlarged paired bones, they cover the dorsolateral nasal capsule. In dorsal view, their posterior proximal three quarters are fused with the sphenethmoid, although with discernable limits. The posterior proximal corner is fused with the

anterodistal corner of the frontoparietals, although with discernable limits. The anterior half does not contact other bones and the nasals are narrowly separated medially (Fig15A, D). In ventral view, they are mostly occluded by the vomers, sphenethmoid, and neopalatines. The anterior edge extends to or slightly over the anterior edge of the anterior process of the vomer (Fig. 15B, E). In lateral view, the nasals present a paraorbital process, which forms the anterior limit of the ocular orbit. The ventral edge of the paraorbital process of the nasals is fused with the dorsal edge of the preorbital process of the maxilla, externally, and the ventral base of the neopalatine, internally.

Frontoparietals — Flat paired bones contributing to the roof of the skull and of approximately the same size of the nasals. (Fig. 15A, D). In dorsal view, they are narrowly (MCP 14490 and MCP 14492) or fully separated medially (MCP 4012 and 14001), leaving a small stripe of the frontoparietal fenestra is exposed. The anteromedial margins of the frontoparietals diverge from one another distally. The distal border of the frontoparietals constitute the upper lateral limit of the orbit and are elevated dorsally, forming a crest that may extend to the posterior limit of the bone. Posteriorly, they contact each other and are fused with the otoccipital.

Parasphenoid — It is cross-shaped and forms the posterior floor of the skull so it is better observed in ventral view (Fig. 15B, E). The long, wide anterior cultriforme process is ornamented on its posterior half with a row of low projections. Anteriorly, the cultriform process overlaps and fuses with the posterior third of the sphenethmoid. The cultriform process is longer than wider; narrows abruptly anterior to the optic fenestra, approximately at half its length, and terminates posterior to the level of the neopalatines, without contact. The parasphenoid alae are relatively short, posterolaterally oriented, fused with the otoccipital, but with their distal edge clearly separated from the proximal edge of the medial ramus of the pterygoid. The posteromedial process of the

parasphenoid is shorter than the cultriforme processes or the alae, acuminated, and fused with the otoccipital.

Vomers —Paired, large-sized, and forming part of the anterior floor of the skull so they are better observed in ventral view (Fig. 15B, E). They are fused posteriorly and separated anteriorly, with a dentigerous process and a laminar anterior region that bears a prechoanal and postchoanal ramus. The dentigerous processes are different between the two species. In *O. planiceps* they are larger, with a broader angle, and bearing 17–18 pedicellate teeth (smaller, narrower angle, and 13–15 pedicellate teeth in *O. vilarsi*). The anterior process is largest and extends nearly to the premaxilla; the margins of the process are rounded. The prechoanal process is short and wide. The poschoanal process is elongated, thin, and with a sharp tip. Dorsally the nasals overlap the vomers.

Premaxillae — Paired, bearing pedicellate teeth in the pars dentalis. The premaxilla has a well-developed alary process that is deflected posteriorly, at approximately at a 30° angle with the maxilla, forming a high and slightly rounded snout in lateral profile. The posteromedial process is longer than the posterolateral. The premaxillae contact the maxilla laterally. Medially, the premaxillae are separated from each other.

Maxillae — Paired, elongated, slightly curved,bearing pedicellate teeth in the pars dentalis. The anterior part of the maxillae slightly overlaps and contacts the premaxillae in dorsal view; the posterior part of the maxillae articulates with the quadratojugals. The maxillae bear a low, broad, and overall rectangular pars facialis, with a simple preorbital process and a shorter paraorbital process. The preorbital process is in contact with the neopalatine and the paraorbital process of the nasal.

Quadratojugals — They are slender and short. The anterior edge is acuminated, and the posterior is expanded and broader. Its anterior tip is overlapped and articulates

with the maxillae, the posterior tip articulates with the ventral ramus of the squamosal.

Mandible — The dentaries are thin and elongated posterolaterally, fused with the relatively conspicuous and quadrangular mentomeckelian bones anteriorly. Posteriorly, the dentaries are superimposed on the anterior third of the angulosplenial, with slight contact between these bones. The angulosplenial reaches and contact the quadratojugal and squamosal (Fig. 15C, F).

Neopalatines —Paired slender bones (Fig. 15B, E). The medial part is sharp and contacts medially with the sphenethmoid. The lateral edge is broader with a slight posteriorly oriented curvature at the end and contacts with the preorbital process of the pars facialis . In their ventral side, each neopalatine bears a crest.

Suspensorium

Pterygoid — Triradiate, Y-shaped, bones (Fig. 15B, E). The pterygoids are in contact with the squamosal and the maxilla. The anterior ramus is long, arched, and anterolaterally oriented, extending through the mandible to about half the ocular orbit. The posterior ramus is slightly longer than the medial ramus. It extends to the mandible, not contacting it, but it contacts with de squamosal. The medial ramus extends almost until the prootics, not contacting it.

Squamosal —T-shaped, with a ventral, otic (posterior), and zygomatic (anterior) rami (Fig. 15C, F). The ventral ramus is longer, and in contact with the posterior ramus of the pterygoid. The zygomatic ramus is slender, with a sharp tip anterior, and anterolaterally oriented. The length of the zygomatic ramus is different between both species. In *O. planiceps* is longer, about twice the length of the otic ramus, while in *O. vilarsi* both rami have about the same length. The otic ramus overlaps and contacts the prootic (Fig. 15A, D).

Axial skeleton

Presacral vertebrae. The presacral region is composed by eight procoelous vertebrae (Fig. 16A, B). The neural arches are well ossified and do not overlap each other (non-imbricated) leaving a broad space between the neural arch of each vertebra and exposing the spinal cord dorsally. The neural arches of vertebrae II, III, and IV bear a spine. The spine of Presacral II is more robust and reaches over Presacral I. Some traces of cartilage are present in the neural spine of each of the first four vertebrae. Transverse processes exhibit different sizes and orientations. Transverse processes of the Presacral II and III are thicker and expanded distally. Transverse processes of Presacral V and VI are of uniform width. Transverse processes of Presacral VII and VIII are thinner distally. The end of the transverse process of Presacral III is cartilaginous and is deflected posteriorly, whereas the ends of the transverse process of Presacral IV–VI are less cartilaginous and are straight. The transverse process of Presacral VII has a small cartilaginous tip. The relative lengths of the transverse processes are different between the two species. In *O. planiceps* is III > VIII > IV > VII > VI > V > II, while in *O. vilarsi* is III> IV > VIII> VI =VII > V > II. Presacral vertebrae VI–VIII have conspicuous prezygapophyses and postzygapophyses. The prezygapophyses of each vertebra articulate through the dorsal facets with the ventral surfaces of the postzygapophyses of the preceding vertebra. Postzygapophyses have a recurved contour in the articular view.

Sacrum and urostyle. The sacrum articulates with Presacral VIII through a pair of prezygapophyses and with the urostyle through a pair of rounded condyles (Fig. 16A, B). The sacral diapophyses are distally expanded and have a dorsal inclination. The distal margins of these diapophyses are thicker and cartilaginous (less so in *O. vilarsi*).

The distal edges of the diapophyses are rounded and overlie the anterior end of the iliac shafts.

The urostyle has a bicondylar articulation with the sacrum; it is long and slender, but shorter than the length of the presacral portion of the vertebral column (Fig. 16A, B). The first third of the urostyle is laterally expanded. Dorsally, it bears a crest along most of its length, which progressively diminishes in height toward its posterior end.

Appendicular skeleton

Pectoral girdle. Arciferal. The procoracoids, epicoracoids, omosternum, and sternum are completely cartilaginous. The ossified elements are coracoids, clavicles, scapulae, and cleithrum (Fig. 16C–F). The clavicles are robust, curved up in the middle, with tips anteromedially oriented, separated from each other. Laterally, each clavicle is fused to the pars acromialis of the scapula and with the glenoid end of the coracoid. The clavicle, coracoid, and scapula form the glenoid fossa. The coracoids are also robust and slightly smaller than the clavicles, with start and end tips equally expanded. In ventral view, the coracoids have a triangular shape process on the distal side of the glenoid end. The scapula is slightly longer and much wider than clavicle. The suprascapular end is equally in size than the zonal end. The cleithrum and ossified portion of the suprascapula are fused. The cleithrum is relatively slender, wider in its anterior margin, growing in length posterolaterally, and in contact with the scapula. The anterior margin of the cleithrum is straight.

Forelimbs. The humerus is the largest bone of the forelimb (Fig. 17C, D). The shaft is slightly curved. The humerus is robust and with well-developed ventral and lateral crests; whereas the medial crest is less developed. The ventral crest extends up to the caput humeri. The distal head (eminentia capitata) is broadly expanded; the glenoid head (caput humeri) is expanded, rounded, and slightly compressed; it is almost equal in

size to the eminentia capitata. The radius and ulna are fused medially, with a middle a groove (sulcus intermedius), to form radio-ulna (Fig. 17G, H). Both ulnar and radial epicondyles are triangular in ventral view. The ulna is slightly longer than the radius, and the distal ulnar epiphysis is more voluminous and wider than the radial epiphysis. The carpus is composed of six individual carpal elements: ulnare, radiale, distal carpal 5-4-3, carpal 2, element y, and prepollex (Fig. 17A, B). The configuration of carpal elements matches the type C morphology. The phalangeal formula is 2–2–3–3. Finger length is IV > V > III > II. The prepollex has a perpendicular orientation. On the female, the prepollex has two elements, including the base.

Pelvic gridle. In dorsal view (Fig. 16 H, J), the configuration of the ilial shafts of the pelvic girdle is a narrow U-shape, which is about twice as wide anteriorly as it is at the base of the shafts. The ilial shaft is simple and are synostotically fused to each other at the proximal ilial corpus. Each shaft bears an ilial crest, more visible at the middle section of the shaft. The dorsal prominence is low, the associated dorsal protuberance is elongated, conspicuous, and positioned above the dorsal margin of the acetabular fossa. The ventral anterior margin of the ventral acetabular expansion is straight and forms an angle of approximately 90° with the ilial shaft. The ilia and ischia are fused to each other. The pubis is completely ossified and forms the ventral portion of the acetabulum. The pubis is completely fused with the ischium and ilium.

Hindlimbs and Pes. The femur is a slim and weakly sigmoid bone, with a rounded caput femoralis that fits into the acetabulum of the pelvic girdle and a bicondylar distal head that articulates with the proximal epiphysis of the tibiofibula (Fig. 18C, D). The femoral crest reaches approximately two fifths of the femur length. The tibiofibula is slightly longer as the femur (Fig. 18E–H). The fusion between tibia and fibulae is only discernible by the presence of a distinct sulcus intermedius (Fig. G,

H). A nutritional foramen perforates the bone diagonally at approximately the midpoint of the diaphysis. The tarsus is composed by five tarsal elements (Fig. 18A, B, I, J): the fibulare, tibiale, distal tarsal 3-2, distal tarsal 1, element Y, and the prehallux. The tibiale and fibulare are elongate, widely separated elements that are fused at the proximal and distal ends (Fig. 18I–J). The phalangeal formula for the foot is 2-2-3-4-3. Toe length is IV > V > III > II > I. The terminal phalanges have a rounded proximal base and a pointy tip.

Comparisons

Due to the newly discovered phenotypic and genetic variation within *Osteocephalus planiceps* and *O. vilarsi*, comparisons between these two species are presented in the Discussion. In this section, we restrict our comparisons to truly diagnostic characters (*i.e.*, known variation does not overlap) among taxa of the *O. planiceps* and *O. taurinus* species group because they have been historically confused (*e.g.*, Trueb & Duellman 1971). *Osteocephalus planiceps* can be distinguished from all the other species of its species group (except *O. vilarsi*) and those of the *O. taurinus* species group as follows (character states of *O. planiceps* in parentheses): Absence of a row of tubercles on the dorsal side of feet (a row of tubercles on the distal edge of Toes IV and V of adult males; Fig. 12), nuptial excrescence in adult males restricted to the base of Finger I (nuptial excrescence of adult males expanding as a line to the base of the finger disc). Besides *Osteocephalus vilarsi*, *O. castaneicola* is the most externally similar species. However, adult males lack vocal sac and slits (both present) and have sparse tubercles on dorsum (heavily tuberculate dorsum), and adult specimens of both sexes lack markings on flanks (at least some dark spots) and have a single distal subarticular tubercle under Finger IV (bifid). Adult males of *O. deridens*, *O. fuscifacies*, and *O. leoniae* are smaller, largest adult male SVL = 35.9 mm, 45.6 mm, and 42.0 mm,

respectively (smallest adult male SVL = 48.9 mm). Additionally, adult males of *O. deridens* and *O. fuscifacies* have a smooth dorsum (densely tuberculate), adults of *O. fuscifacies* lack a subocular white spot (present), and adults of *O. leoniae* lack markings of flanks (present) and have a bicolored iris, upper half pale and lower half darker (golden with black reticulations). *Osteocephalus taurinus* is further differentiated by having a head wider than long (longer than wide) and lacking a white subocular spot (present).

Distribution and habitat

We report on 14 localities with voucher specimens of *Osteocephalus planiceps* sensu this work (Fig. 2, Appendix 4). All identifications are confirmed by DNA sequences except that of the holotype. Although a search on GBIF on 22 February 2022 retrieved 362 records with coordinates (265 with preserved specimens), our results indicate that identifying specimens of *O. planiceps* from congeneric species, particularly *O. castaneicola* and *O. vilarsi*, is difficult. Thus, rather than incorporating potential identification errors from other databases, we prefer to use identifications corroborated by the analysis of DNA sequences. Undoubtedly, future studies will report occurrences in new localities, although we think that the localities that we herein report provide a good summary of the current knowledge on the distribution of *O. planiceps* considering the geographic scale at hand (Fig. 2).

According to our confirmed records, *O. planiceps* is restricted to the western Amazonian lowlands (103–700 m a.s.l.). The northernmost locality is in Caquetá, Colombia, about 1,150 km in straight line from the southernmost one in Imiria, Loreto, Peru. The westernmost locality is in Ecuador, about 915 km in straight line from the easternmost one in Leticia, Amazonas, Colombia. Our confirmed records correspond to localities distributed across Brazil, Colombia, Ecuador, and Peru. To the best of our

knowledge, our study provides the first confirmed record of *O. planiceps* from Brazil, represented by two specimens from Mata Infraero, Acre, on the western margin of the Yuruá River (Fig. 2; Appendix 4). We were only able to confirm two localities from Colombia, but we refer to Lynch (2008), Suárez-Mayorga & Lynch (2017), and Medina-Rangel *et al*. (2019) for other potential localities. Nonetheless, considering the proximity of several Brazilian localities of *O. vilarsi* to the Colombian border, it is very likely that some of the Colombian records reported in the aforementioned literature actually correspond to *O. vilarsi*. In Ecuador, we report localities from the provinces of Napo, Orellana, and Sucumbios. However, this species seems to be more widely distributed within Ecuadorian Amazonia. A search on 22 February, 2022 using BioWeb (2021) reported 359 specimens from different localities including the provinces of Morona Santiago, Pastaza, and Zamora Chinchipe, besides the aforementioned ones. Within Peru, we confirmed six localities within the departments of Loreto and Ucayali, all along the axis of the Ucayali River (Fig. 2). The distribution of *O. planiceps* within Peru is certainly larger, as confirmed by trustworthy literature records (*e.g.*, Duellman & Mendelson, 1995).

We have collected specimens of *Osteocephalus planiceps* from a variety of lowland Amazonian rainforests in different states of preservation. Specifically, we have found *O. planiceps* in both terra-firme (non-flooded) and Várzea (seassonally flooded) forests, although it seems more abundant in the former. Among terra-firme forests, Gagliardi-Urrutia (2020) reported its presence on both white-sand and clay dominant soil forests at three localities in Loreto, Peru (EBJAA, CIJH, and Frontera; Fig. 14). However, the species is more abundant in forests growing on soils with a dominant proportion of sand (Gagliardi-Urrutia 2020). We have encountered *O. planiceps* in highly disturbed forests in the vicinity of human settlements and in well-preserved

primary forests. We have never recorded this species from open habitats such as savannas or relatively forest clearings, although it can be found on the vegetation limiting open environments. We always found specimens of *O. planiceps* perching on vegetation or structures elevated above the ground, as low as 0.5 m, and there reports of specimens from 25 m in the forest canopy (Guayasamin *et al*. 2006).

Natural history

The reproductive biology of *O. planiceps* is puzzling because despite its abundance and detectability in many localities, we still lack basic information and most of what it is known derives from rather anecdotic field observations. Our field experience indicate that adult specimens become particularly elusive while reproducing, which combined with their apparent preference for sites high in the forest canopy probably explain the lack on data. Most field observations report males vocalizing from phytotelmata, particularly from bromeliads high on the canopy (Guayasamin *et al*., 2006; Ron 2011). One of us (SC-F) observed two males vocalizing at different dates in Leticia, Colombia, on December 2009. One was inside a hollow cut trunk, although still rooted and standing, filled by water. The trunk was about 1 m in diameter and height. The other one was perched on the edge of a 100 l plastic bucket of 1 m height placed on the ground to collect rain water on a biological station. Surprisingly, Read & Ron (2018) reported on males from Ecuador vocalizing while perching on low vegetation surrounding swamps and flooded areas and on a single specimen vocalizing while floating on the water. One of us (PT) heard several males vocalizing about 1.20 m above the flooded forest floor at CIJH, Loreto, Peru (Fig. 14). An active search on the lower strata vegetation surrounding the temporal pond resulted in the collection of three adult males sexually active as inferred from expanded vocal sacs and numerous keratinized spines on dorsum. In nature, there are reports of tadpoles found in the water

stored of the axils of bromeliads together with vocalizing males and fertilized eggs (Guayasamin *et al*., 2006; Ron 2011). Among the specimens that we have directly examined, there are two females with externally visible eggs in the gonads. We dissected the specimen MCP 14001 (SVL = 61.7 mm) and counted 876 eggs. The eggs are small (1.4–1.7mm (1.6 ± 0.1, n= 10 eggs)), with just the animal pole pigmented. Reproductive aspects such as adult site fidelity, parental care, tadpole morphology, or oophagia, which have been reported for other congeneric species using phytotelmata for reproduction (*e.g*., Jungfer & Schiesari, 1995; Ferrão *et al*., 2019), are unknown for *O. planiceps*.

The advertisement call of *Osteocephalus planiceps* consists on a series of 1–4 short "quacks" sounds separated by short silences (< 0.5 s) that to the human ear are reminiscent of the caricaturized vocalization of a monkey used in western popular culture. Although their call is commonly heard by herpetologist working in Amazonian lowland forests, it is rarely recorded. There are only two quantitative descriptions on the literature. Ron & Pramuk (1999) described the advertisement call based of two recorded calls from a single male vocalizing from a bromeliad in Loreto, Peru. Ferrão *et al*. (2019) described the call based on a total of 19 advertisement calls from three different males from Napo and Orellana. Pooled data from both descriptions shows that the call lasts 108–608 ms, having 1–4 notes, with each note lasting 58–108 ms and separated by silent intervals of 34–155 ms. The dominant frequency is 323–1162 Hz with no evident signs of frequency modulation, although the amplitude is weakly modulated reaching its peak in the middle section of each note (Ferrão *et al*., 2019: Fig. 9D, E).

Osteocephalus planiceps is known from western Amazonia, the most species rich region in the world with reports of > 100 spp in a few km^2 (Lynch 2005; Bass et al., 2010). Thus, this species occurs in sympatry with several dozens of other anuran

species, including many other hylids. Congeneric species known to occur in sympatry include, but are not restricted to, *O. buckleyi*, *O. cabrerai*, *O. deridens*, *O. heyeri*, and *O. taurinus*.

Discussion

Species delimitation between *Osteocephalus planiceps* and *O. vilarsi*. As diagnostic phenotypic characters (*i.e*., known variation not overlapping) supporting the differentiation between *O. planiceps* and *O. vilarsi*, Ferrão *et al*. (2019) listed (characters of the latter species in parentheses): (1) color of tibiofibular and femur bones in life green (white), (2) color of iris in metamorphs with black reticulation, upper portion with red pigmentation on yellow ground and lower iris tan with red pigmentation near the pupil (entirely bright red without black reticulation), (3) two-notes call duration of 198–259 ms (144–180 ms), (4) three-notes call duration 360–465 ms (162–337 ms), (5) and non-overlapping morphometric space among adult females in PCA analysis. Below we discuss these characters in light of our results.

We find intraspecific polymorphism in tibiofibular and femur bones in life (Fig. 11) in *O. planiceps* from three different localities. Furthermore, the polymorphism is neither exclusive of a sex or developmental stage. Ferrão *et al.* (2019), based on photos, reported on a single specimen from Ecuador with white bones. Our discovery demonstrate that white bones are much frequent in *O. planiceps* than previously suggested. We report that the color of iris in metamorphs of *O. planiceps* is entirely bright red without black reticulation and identical to that described for *O. vilarsi* (Fig. 6A, B). The difference reported by Ferrão *et al*. (2019) stemmed from comparing metamorphs of *O. vilarsi* with a juvenile of *O. planiceps* (Ferrão *et al*. 2019: Fig. 3D, H). In other words, as clearly illustrated in our Figure 6, Ferrão *et al*. (2019) were comparing characters that vary with development between different developmental

stages. Although we do not analyze new call data from either species, the differences in call duration reported by Ferrão *et al*. (2019) are problematic: (i) advertisement call duration does broadly overlap (108–608 ms in *O. planiceps* versus 144–337 ms in *O. vilarsi*), (ii) the non-overlapping differences correspond to less than 30 ms, which are difficult to interpret as facilitating reproductive isolation when the call duration within either of those species vary much more, and (iii) this small differences are based on very small sample sizes (n = 3 specimens of each species). Finally, we demonstrate that the morphospace of both species broadly overlap when summarized in PCAs, both considering SVL and removing its influence. We argue that the differences in morphospace reported by Ferrão *et al*. (2019) were a consequence of their small sample size of specimens of *O. planiceps* (n = 8 females and 3 males). In summary, the variation of all putatively diagnostic characters overlap between *O. planiceps* and *O. vilarsi*, except for those related with call duration, which are based on comparing subdivisions of the character and report gaps of < 30 ms inferred from a very limited sample size.

Regardless of phenotypic differentiation, support for the recognition of *Osteocephalus planiceps* and *O. vilarsi* comes from the phylogenetic results of Jungfer *et al*. (2013), Ferrão *et al*. (2019), and Blotto *et al*. (2020). None of their analyses recovered *O. planiceps* and *O. vilarsi* as each other closest relatives, implying that evolutionary history is not compatible with a single evolutionary lineage (Fros & Kluge 1994). Thus, their situation would mirror that of the treefrog species *Phyllomedusa camba* and *P. chaparroi* (Castroviejo-Fisher *et al*. 2017). However, our results challenge this scenario because we recover *O. planiceps* and *O. vilarsi* as sister groups (Fig. 3B). This new result is unlikely to be caused by gene sampling, inasmuch as we used the same markers than the most complete study to date (Blotto *et al*. 2020), or

choice of optimality criterion because Jungfer *et al*. (2013), Ferrão *et al*. (2019), and Blotto *et al*. (2020) also used ML or Bayesian analysis. We argue that the key factor is our increased sampling within the *O. planiceps* species group, which added previously unknown haplotypes of both species. We acknowledge the low BS (< 50) for the most exclusive clade containing *O. planiceps* and *O. vilarsi* in our results, but the BS or posterior clade probabilities reported to support a different relationship between these two species are also low (Jungfer *et al*. 2013; Ferrão *et al*. 2019; and Blotto *et al*. 2020). In any case, the sister relationship of *O. planiceps* and *O. vilarsi* does not per se invalidate their taxonomic status. For example, Escalona *et al*. (2021) recognized as two different species of *Boana* (Hylidae) two reciprocally monophyletic and sister clades with low divergence and BS support, which is similar to our phylogenetic results for *O. planiceps* and *O. vilarsi*. However, they argued that the supporting evidence for their conclusion was not on the phylogenetic results, which could be easily interpreted as more compatible with variation within a species, but on diagnostic phenotypic characters observed on a large sample of specimens from multiple localities and the existence of a geographic barrier that contributed to isolation (each delimited species occurs on opposite sides of the Orinoco River). Although our phylogenetic result somehow mirrors those of Escalona *et al*. (2019, 2021), our evaluation of phenotypic characters does not. Thus, the evidence at hand seems to tip the scale towards a single species with a wide distribution.

By studying for the first time the ossified skeleton of both species, we discover four potential diagnostic characters (states of *O. vilarsi* in parenthesis): (1) rhombus-shape sphenethmoid in dorsal view (pentagon-shape), (2) dentigerous process of vomer larger, with a broader angle, and bearing 17–18 pedicellate teeth (smaller, narrower angle, and 13–15 pedicellate teeth), (3) zygomatic ramus of the squamosal about twice

the length of the otic ramus (about the same length), and (4) relative lengths of the transverse processes of presacral vertebrae III > VIII > IV > VII > VI > V > II (III> IV > VIII> VI =VII > V > II). However, one needs to keep in mind that our sampling size, although larger than most osteological species comparisons in the anuran literature, is still limited (*O. planiceps*, n = 3 females and 1 male from three localities; *O. vilarsi* = 4 females and 1 male from three localities) for species that are distributed across hundreds of kilometers and important geographic areas such as large Amazonian rivers. As we show herein with bone coloration, morphospace, or DNA sequences increasing sampling size from a handful of specimens to a couple of dozens can drastically change our perception of character variation.

In light of the new evidence presented in our study, it is pertinent to evaluate if *O. planiceps* and *O. vilarsi* should be recognized as different species. In other words, is the observed variation better explained as intraspecific polymorphism of a widely distributed evolutionary lineage or as two independently evolving groups of populations? We argue that these two hypotheses are defendable with the current evidence. This is often the case with organisms with wide distributions across geographic barriers and contact zones. For example, Ruane *et al*. (2014) and Burbrink & Guiher (2015) recognized several species of snakes, while with the same data, Chamber & Hillis (2020) and Hillis (2019, 2020) did not. Additional data and analysis revealed a complex scenario of isolation and divergence, secondary contact and introgression (Burbrink *et al.* 2021). As in the examples mentioned above, one will need to improve the geographic sampling, particularly for specimens from the interfluves of the Ucayali, Putumayo, Caquetá, Apaporis, and Vaupés rivers in Colombia, where specimens of *O. planiceps* and *O. vilarsi* most likely enter in contact. Furthermore, one will need to scalete the genetic data to a genomic scale, so that different scenarios of isolation,

contact, and geneflow could be evaluated. Until that time, we prefer to maintain both species on the basis of their so far unchallenged reciprocal monophyly and newly discovered osteological diagnostic characters. However, we want to underscore that the taxonomic status of *O. vilarsi* as a different species from *O. planiceps* is very unstable

Species diversity within the *Osteocephalus leprieurii* species group. As currently understood, the *O. leprieuri* species group includes two described species (*i.e.*, *O. leprieuri* and *O. yasuni*) and a candidate new species from the rio Abacaxis, Amazonas, Brasil (Jungfer *et al*. 2013; Blotto *et al*. 2020). Our phylogenetic results indicate that a specimen (MCP 14487) from Frontera, Loreto, Peru, is sister to all this taxa (Fig. 3B). Furthermore, its genetic distance with specimens of the other two species are 2.2–4.2 %, which are larger than among specimens of *O. leprieurii* and *O. yasuni*. These results flag specimen MCP 14487 as a representative of a new species. Unfortunately, the specimen is a juvenile and despite our sampling efforts at this locality, we have been unable to secure other individuals. Another noteworthy result is our report of *O. yasuni* from the south and north margins the Japura River, Amazonas, Brazil. This represents the northernmost locality for the species and the second record from Brazil. Finding *O. yasuni* at this locality also opens and intriguing taxonomic issue. Melin (1941) described *Hyla leprieurii britti* from Rio Uaupés (north of the Rio Japú), Amazonas, Brazil, stating that it resembles a good deal *O. leprieurii* (*Hyla* at the time). Trueb & Duellman (1971) studied the holotype of the subspecies and a large series of *O. leprieurii* from different countries and considered the former taxon a junior synonym of the latter. Ron & Pramuk (1999) described *O. yasuni* from the Amazonian lowlands of Ecuador focusing on differentiating it from *O. planiceps*, according to them the most similar species within the area. Ron & Pramuk (1999) differentiated *O. yasuni* from *O. leprieurii* (character states of the latter in parentheses) by having irregular black

reticulations in a bronze iris (straight black lines radiating from the pupil), absence of well-defined transverse brown marks on the dorsum (present), absence of pale stripes on the heels and around the cloacal opening (present), lack the frontoparietal fenestra (present according to Trueb and Duellman,1971). Jungfer & Hödl (2002) redescribed *O. leprieurii* on the basis of fresh material and field observations from French Guiana and concluded that *O. leprieurii* most closely resembles *O. yasuni* and that the latter species is only different by having fewer dorsal spines in males and lacking subdigital nuptial excrescences. Both characters, however, may depend on the breeding condition of the specimen at the time of preservation. In the same study, Jungfer & Hödl (2002) also reported on differences between the only known specimen of *Hyla leprieurii britti* and their newly characterized *O. leprieurii*. Using phylogenetic analysis of DNA sequences, Jungfer *et al*. (2013) showed that the phenotypic variation assigned to *O. leprieurii* by Trueb & Duellman (1971) actually corresponds to more than one species. Our discovery of *O. yasuni* on both margins of the Japurá River is relevant because these localities are within the region from which *Hyla leprieurii britti* was collected and demonstrates that the large northern affluents of the Amazonas River are not an efficient barrier for *O. yasuni*. Given the close phenotypic similarity between *O. leprieurii*, *O. yasuni*, and *Hyla leprieurii britti*, and the sister phylogenetic relationship combined with low genetic divergence between *O. leprieurii* and *O. yasuni*, it seems likely that either *Hyla leprieurii britti* is a valid species of *Osteocephalus* and *O. yasuni* is its junior synonym or that these three names refer to the same species and the name *Osteocephalus leprieurii* has priority over the other two. We recommend further studies before implementing nomenclatural changes.

Variation of bone coloration in *Osteocephalus*. The green-blue coloration of bones and other tissues in frogs is caused by high concentrations of the pigment biliverdin (Barrio 1965; Taboada *et al*. 2020). This character is known for more than 430 anuran species among 11 families (Arthroleptidae, Centrolenidae, Craugastoridae, Hemiphractidae, Hylidae, Hyperoliidae, Limnodynastidae, Mantellidae, Myobatrachidae, Ranidae, and Rhacophoridae). Bone coloration is largely considered as a fixed character within species (*i.e*., no intraspecific polymorphism) and consequently used in anuran systematics (e.g., Centrolenidae; Guayasamin *et al*., 2009; Castroviejo-Fisher *et al.* 2011). In *Osteocephalus* green bones have been reported for several species (Ron & Pramuk 1999; Jungfer *et al*. 2000; Jungfer & Lehr 2001; Jungfer & Hödl 2002; Moravec *et al*. 2009; Jungfer 2010; Ron *et al*. 2010; Ron *et al.* 2012; Chasiluisa *et al*. 2020; Melo-Sampaio *et al*. 2021) and is probably one of the few groups with reported intraspecific variation. For example, bone color is associated with development in *O. leprieurii* and *O. yasuni* because green bones in juveniles become white in adults (Jungfer & Hödl 2002; Cisneros-Heredia 2007). Bone color is also polymorphic in adults of *O. castaneicola*, although their link to development is unknown because the character has not been described for metamorphs or juveniles (Moravec *et al.* 2009).

Ours results demonstrate bone color polymorphism in both adults and juveniles of *O. planiceps*, probably being the first case of non-ontogenic intraspecific polymorphism in anuran bone color. Of 45 specimens examined, bone color varied within sex, developmental stage, and geographic location (Table 5). The variation in bone color of *O. planiceps* in combination with the fact that it is a commonly encountered species suggests that it could be a model organism to further address the fascinating but complicated genetic and enviromental basis of bone coloration in anurans (Taboada *et al.* 2020). Our discovery also offers important lessons for

Osteocephalus systematics. Many studies have used bone color in life as a diagnostic character (*e.g*., Ron & Pramuk, 1999; Jungfer 2010; Ferrão *et al*. 2019), but its value needs to be pondered on the basis of its intraspecific variation.

Skeletal characters. Externally evident frontoparietal ridges are rare in anurans; consequently, their presence have drawn the attention of researchers. To our knowledge, they are not linked to any function and its formation is likely a byproduct of skull hyperossification. Their variation have a long pedigree in *Osteocephalus* systematics. For example, Trub & Duellman (1971) used the shared presence of frontoparietal ridges as evidence to synonymize *O. planiceps* under *O. taurinus* and their variation is commonly used in species descriptions as a diagnostic feature (Ron & Pramuk 1999; Jungfer & Lehr 2001; Jungfer 2010; Jungfer 2011; Jungfer *et al*. 2016). However, although it is well-known that it is an intraspecific variable character in at least some species (*e.g*., Trub & Duellman 1971; Jungfer 2010), its variation is hardly mentioned in the literature, with even contradictory descriptions. For example, while in *O. buckleyi* frontoparietal ridges are reported as absent (Jungfer 2010), distinctive ridges through the skin are described for its junior synonym *O. vilmae* (Ron *et al*. 2012).

We evaluated its variation relation with developmental stage, sex, and size (Fig. 19) in both *O. planiceps* e *O. vilarsi*. Our results clearly indicate an link with ontogeny, because only adult specimens may present this structure. Both sexes may have frontoparietals ridges, but most males only develop low ridges. Size is also positively related with the presence and development of this structure as it is also non-independent from sex and ontogeny. The large observed variation in the presence and degree of development of frontoparietals ridges among adult specimens of the same sex and size indicate that other factors are at play. For example, internal and external factors such as genetic variation and diet, a diet. As in the case of bone coloration, morphometrics, and

other aforementioned characters, the presence and level of development of frontoparietal ridges should be used with caution in *Osteocephalus* systematics and only in reference to their variation.

Our osteological descriptions reveal a previously unreported process in the coracoid (Fig. 16C–F). To evaluate their presence in other closely related taxa and their potential synapomorphic value, we checked 3D osteological models derived from CT-scans of specimens of *Osteopilus septentrionalis*, *Phyllodytes sp*., *Tepuihyla shushupe*, and *T. tuberculosa*. All taxa except *Phyllodytes sp*. have the coracoid process, indicating that its presence is a potential synapomorphy of the most exclusive clade containing *Dryaderce*s, *Osteocephalus*, *Osteopilus*, *Phyllodytes*, and *Tepuihyla*. However, its variation across hylids needs to be further investigated to determine at which level of universality this character is informative.

Acknowledgements. We thank Omar Rojas-Padilla and Maria Eduarda Appel for help during field work. We are thankful to the inhabitants of the Frontera community for their hospitality, especially the family Pacay DaSilva ,who sheltered us in their house. We thank Juliano Romanzini for technical support at MCT-PUCRS. We are thankful to F.P. Werneck (INPA-H) and Ned Gilmore (ANSP) for allowing us to study material under her care. PT received final support from CAPES (process 42005019002P7).

References

Barrio, A. (1965) Cloricia fisiológica en batracios anuros. *Physis* 25, 137–142.

Bass, M.S., Finer, M., Jenkins, C.N., Kreft, H., Cisneros-Heredia, D.F., McCracken, S.F., Pitman, N.C.A., English, P.H., Swing, K., Villa, G., Di Fiore, A., Voigt, C.C. & Kunz, T.H. (2010) Global conservation significance of Ecuador's Yasuní National Park. *PLoS ONE* 5. https://doi.org/10.1371/journal.pone.0008767

BioWeb. Pontificia Universidad Católica del Ecuador. (2021) Base de datos de la colección de anfibios del Museo de Zoología QCAZ. Versión 2021.0. Available at https://bioweb.bio/portal/

Blotto, B.L., Lyra, M.L., Cardoso, M.C.S., Trefaut Rodrigues, M., R. Dias, I., Marciano-Jr, E., Dal Vechio, F., Orrico, V.G.D., Brandão, R.A., Lopes de Assis, C., Lantyer-Silva, A.S.F., Rutherford, M.G., Gagliardi-Urrutia, G., Solé, M., Baldo, D., Nunes, I., Cajade, R., Torres, A., Grant, T., Jungfer, K.H., da Silva, H.R., Haddad, C.F.B. & Faivovich, J. (2020) The phylogeny of the Casque-headed Treefrogs (Hylidae: Hylinae: Lophyohylini). *Cladistics*, 1–37. https://doi.org/10.1111/cla.12409

Boulenger, G.A. (1882) *Catalogue of the Batrachia Salientia s. Ecaudata in the collection of the British Museum*. Ed. 2., (reprinted: Wheldon & Wesley, ltd. and Verlag J. Cramer, 1966), London, 503 pp.

Brower, A.V. (2018) Going rogue. *Cladistics*, 34:467–468. doi:10.1111/cla.12211

Burbrink, F. T., Bernstein, J. M., Kuhn, A., Gehara, M. & Ruane, S. (2021) Ecological divergence and the history of gene flow in the Nearctic milksnakes (Lampropeltis triangulum complex). *Systematic Biology*. https://doi.org/10.1093/sysbio/syab093

Burbrink, F.T. & Guiher, T.J. (2015) Considering gene flow when using coalescent methods to delimit lineages of North American pitvipers of the genus Agkistrodon. *Zoological Journal of the Linnean Society*. 173:505– 526.

Carvalho, M.D.A., Luiz, P., Peloso, V. & Sturaro, M.J. (2017) On the distribution of *Osteocephalus castaneicola* Moravec, Aparicio, Guerrero-Reinhard, Calderón, Jungfer & Gvoždík, 2009 (Anura: Hylidae), with new records for Amazonian Brazil. *Herpetology Notes*, 10, 593–596.

Castroviejo-Fisher, S., Vilà, C., Ayarzagüena, J., Blanc, M. & Ernst, R. (2011) Species diversity of Hyalinobatrachium glassfrogs (Amphibia: Centrolenidae) from the Guiana Shield, with the description of two new species. *Zootax*, 3132(1), 1–55.

Chambers, E.A. & Hillis, D.M. (2020) The multispecies coalescent over-splits species in the case of geographically widespread taxa. *Systematic Biology*. 69:184–193.

Chasiluisa, V.D., Caminer, M.A., Varela-Jarmillo, A. & Ron, S.R. (2020) Description and phylogenetic relationships of a new species of treefrog of the *Osteocephalus buckleyi* species group. *Neotropical Biodiversity*, 6(1), 21–36.

Cisneros-Heredia, D. F. (2007) Notes on some *Osteocephalus* treefrogs from Amazonian Ecuador. *Herpetozoa* 19:183.

Cope, E. D. (1874) On some Batrachia and Nematognathi brought from the upper Amazon by Prof. Orton. *Proceedings of the Academy of Natural Sciences*, 25, 120–137.

Duellman, W.E. & Mendelson, J.R. (1995) Amphibians and reptiles from northern Departamento Loreto, Peru: taxonomy and biogeography. *University* of *Kansas Science Bulletin*, 55: 329-376.

Duellman, W.E. & Trueb, L. (1986) *Biology of amphibians*. McGraw-Hill Book Company, New York, St. Louis, San Francisco.

Duellman, W.E. (1970) Hylid frogs of Middle America. *Monograph of the Museum of Natural History, the University of Kansas*, 1: 1-753.

Duellman, W.E. (2019) The last one: A new species of *Osteocephalus* (Anura: Hylidae)

from Colombia, with comments on the morphological and behavioral diversity within the genus. *Phyllomedusa* 18, 141–157. https://doi.org/10.11606/issn.2316-9079.v18i2p141-157

Duméril, A.M.C. & Bibron, G. (1841) *Erpétologie générale ou histoire naturelle compléte des reptiles*, Vol. 8. Paris.

Edgar, R.C. (2004) MUSCLE: a multiple sequence alignment method with reduced time and space complexity. BMC *Bioinformatics*, 5: 113.

Escalona, M., Juncá, F.A., Giaretta, A.A., Crawford, A.J. & La Marca, E. (2019) Contrasting genetic, acoustic, and morphological differentiation in two closely related gladiator frogs (Hylidae: *Boana*) across a common Neotropical landscape. *Zootaxa*, 4609, 519–547. https://doi.org/10.11646/zootaxa.4609.3.8

Escalona, M., La Marca, E., Castellanos, M., Crawford, A.J., Rojas-Runjaic, F.J.M., Giaretta, A.A., Señaris, J.C. & Castroviejo-Fisher, S. (2021) Integrative taxonomy reveals a new but common Neotropical treefrog, hidden under the name *Boana xerophylla*. *Zootaxa*, 4981, 401–448. https://doi.org/10.11646/zootaxa.4981.3.1

Fabrezi, M. (1992) El carpo de los anuros. *Alytes*, 10: 1–29.

Fabrezi, M. (1993) The anuran tarsus. *Alytes*, 11: 47–63.

Fabrezi, M. (2001) A survey of prepollex and prehallux variation in anuran limbs. *Zoological Journal of the Linnean Society*, 131: 227–248.

Ferrão, M., Moravec, J., Moraes, L.J.C.L., de Carvalho, V.T., Gordo, M. & Lima, A.P. (2019) Rediscovery of *Osteocephalus vilarsi* (Anura: Hylidae): An overlooked but widespread Amazonian spiny-backed treefrog. *PeerJ*, 1–35. https://doi.org/10.7717/peerj.8160

Frost, D. R. & Kluge, A. G. (1994) A consideration of epistemology in systematic biology, with special reference to species. *Cladistics*, 10(3), 259-294.

Frost, D.R. (2022) Amphibian Species of the World: an Online Reference, version 6.1, Eletroic Database American, Museum of Natural History, New York, USA. Available from: at https://amphibiansoftheworld.amnh.org/index.php. (accesed 12 January 2022).

Gagliardi-Urrutia, G. (2020) El papel de los bosques de arena blanca en la diversidad de anfibios de la Amazonia Oeste. Ph. D. dissertation, Pontifícia Universiade Católica do Rio Grande do Sul.

Gómez, R.O. & Turazzini, G.F. (2016) An overview of the ilium of anurans (Lissamphibia, Salientia), with a critical appraisal of the terminology and primary homology of main ilial features. *Journal of Vertebrate Paleontology,* 36: e1030023.

Gordo, M. & Neckel-Oliveira, S. (2004) *Osteocephalus planiceps*. *Herpetological Review,* 35:79.

Guayasamin, J. M., Castroviejo-Fisher, S., Trueb, L., Ayarzagüena, J., Rada, M. & Vilà, C (2009) Phylogenetic systematics of Glassfrogs (Amphibia: Centrolenidae) and their sister taxon Allophryne ruthveni. *Zootaxa*.

Guayasamin, J. M., Ron, S. R., Cisneros-Heredia, D. F., Lamar, W. W., McCracken, S. F. (2006) A new species of frog of the *Eleutherodactylus lacrimosus* assemblage (Leptodactylidae) from the western Amazon Basin, with comments on the utility of canopy surveys in lowland rainforest. *Herpetologica*, 62:191-202.

Hillis, D.M. (2019) Species delimitation in herpetology. *Journal of Herpetology*. 53:3–12.

Hillis, D.M. (2020) The detection and naming of geographic variation within species. *Herpetological Review*. 51:52–56.

Jungfer K-H. (2010) The taxonomic status of some spiny-backed treefrogs, genus *Osteocephalus* (Amphibia: Anura: Hylidae). *Zootaxa,* 2407(1):28–50 DOI

10.11646/zootaxa.2407.1.2.

Jungfer, K., Ron, S.R., Seipp, R. & Almendáriz, A. (2000) Two new species of hylid frogs, genus *Osteocephalus*, from Amazonian Ecuador. *Amphibia Reptilia*, 21.

Jungfer, K.-H. & Hödl, W. (2002) A new species of *Osteocephalus* from Ecuador and a redescription of *O. leprieurii* (Duméril & Bibron, 1841) (Anura: Hylidae). *Amphibia-Reptilia*, 23, 21–46.

Jungfer, K.-H. & Lehr, E. (2001) A new species of *Osteocephalus* with bicoloured iris from Pozuzo (Peru: Departamento de Pasco) (Amphibia: Anura: Hylidae). *Zoologische Abhandlungen Staatliches Museum für Tierkunde Dresden*, 51, 321–329.

Jungfer, K.-H. & Schiesari, L.C. (1995) Description of a central Amazonian and Guianan tree frog, genus *Osteocephalus* (Anura, Hylidae), with oophagous tadpoles. *Alytes*, 13, 1–13.

Jungfer, K.-H. (2015) Taxonomy and Systematics of Spiny-Backed Treefrogs, Genus *Osteocephalus* (Amphibia: Anura: Hylidae)., 275.

Jungfer, K.H., Faivovich, J., Padial, J.M., Castroviejo-Fisher, S., Lyra, M.M., V. M. Berneck, B., Iglesias, P.P., Kok, P.J.R., Macculloch, R.D., Rodrigues, M.T., Verdade, V.K., Torres Gastello, C.P., Chaparro, J.C., Valdujo, P.H., Reichle, S., Moravec, J., Gvoždík, V., Gagliardi-Urrutia, G., Ernst, R., De la Riva, I., Means, D.B., Lima, A.P., Señaris, J.C., Wheeler, W.C. & F. B. Haddad, C. (2013) Systematics of spiny-backed treefrogs (Hylidae: *Osteocephalus*): An Amazonian puzzle. *Zoologica Scripta*, 42, 351–380. https://doi.org/10.1111/zsc.12015

Kalyaanamoorthy, S., Minh, B.Q., Wong, T.K.F., von Haeseler, A. & Jermiin, L.S. (2017) ModelFinder: Fast model selection for accurate phylogenetic estimates. *Nature Methods*, 14:587-589. https://doi.org/10.1038/nmeth.4285

Kearney, M. (2002). Fragmentary taxa, missing data, and ambiguity: mistaken assumptions and conclusions. Systematic biology, 51(2), 369-381.

Kok, P.J. & Castroviejo-Fisher, S. (2008) Glassfrogs (Anura: Centrolenidae) of Kaieteur National Park, Guyana, with notes on the distribution and taxonomy of some species of the family in the Guiana Shield. *Zootaxa*, 1680, 25-53.

Larsson, A. (2014) AliView: a fast and lightweight alignment viewer and editor for large datasets. *Bioinformatics*, 30: 3276–3278.

Lynch, J. D. (2005) Discovery of the richest frog fauna in the world—an exploration of the forests to the north of Leticia. *Revista de la Academia Colombiana de Ciencias Exactas, Fisicas y Naturales*, 29, 581–588.

Lynch, J. D. (2008) *Osteocephalus planiceps* Cope (Amphibia: Hylidae): its distribution in Colombia and significance. *Revista de la Academia Colombiana de Ciencias Exactas, Fisicas y Naturales*, 32, 87–91.

Lyra, M. L., Haddad, C. F. B., & Azeredo-Espin, A. M. L. (2017) Meeting the challenge of DNA barcoding Neotropical amphibians: Polymerase chain reaction optimization and new COI primers. *Molecular Ecology Resources*, 17, 966–980. DOI: 10.1111/1755-0998.12648

Malnate, E. V. (1971) A catalog of primary types in the herpetological collections of the Academy of Natural Sciences, Philadelphia (ANSP). *Proceedings of the Academy of Natural Sciences of Philadelphia,* 123: 345–375.

Medina-Rangel, G. F., Méndez-Galeano, M. A. & Calderón-Espinosa, M. L. (2019) Herpetofauna of San José del Guaviare, Guaviare, Colombia. *Biota Colombiana*, 20(1), 75-90. DOI: 10.21068/c2019.v20n01a05.

Melin, D. (1941) Contribution to the knowledge of Amphibia of South America. *Göteborgs Kungl. Vetensk. o. Vitterh. Samh. Handl*, Föl. 6, Ser. B, 1: 1-71.

Melo-Sampaio, P. R., Ferrão, M. & Moraes, L.J.C. (2021) A new species of *Osteocephalus Steindachner*, 1862 (Anura, Hylidae), from Brazilian Amazonia. *Breviora*, 572: 1–21. DOI: 10.3099/0006-9698-572.1.1

Minh, B.Q., Schmidt, H.A., Chernomor, O., Schrempf, D., Woodhams, M.D., von Haeseler, A. & Lanfear, R. (2020) IQ-TREE 2: New models and efficient methods for phylogenetic inference in the genomic era. *Molecular Biology and Evolution*, 37:1530-1534. https://doi.org/10.1093/molbev/msaa015

Moravec, J., Aparacio, J., Guerrero-Reinhard, M., Calderón, G., Jungfer, K. & Gvozdik, V. (2009) A new species of *Osteocephalus* (Anura: Hylidae) from Amazonian Bolvia: frist evidence of tree frog breeding in fruit capsules of Brazil nut tree. *Zootaxa*, 2215, 37-54.

Moura, P. H. A. G., Elias-Costa, A. J., Nunes, I., & Faivovich, J. (2021) Diversity and evolution of the extraordinary vocal sacs of casque-headed treefrogs (Anura: Hylidae). *Biological Journal of the Linnean Society*, Volume 134, Issue 2, October 2021, Pages 423–442, https://doi.org/10.1093/biolinnean/blab083

Myers, C.W. & Duellman, W.E. (1982) A new species of Hyla from Cerro Colorado, and other tree frog records and geographical notes from western Panama. *American Museum Novitates*, 2752: 1-32.

Palumbi, S., Martin, A., Romano, S., McMillan, W.O., Stice, L. & Grabowski, G. (1991) *The simple fool's guide to PCR. Version 2*, University of Hawaii, Honolulu, 47 pp.

Read, M. & Ron, S. R. (2018) *Osteocephalus planiceps* En: Ron, S. R., Merino-Viteri, A. Ortiz, D. A. (Eds). Anfibios del Ecuador. Version 2021.0. Museo de Zoología, Pontificia Universidad Católica del Ecuador. https://bioweb.bio/faunaweb/amphibiaweb/FichaEspecie/Osteocephalus%20planiceps, (accessed 25 February 2022)

Ron, S. R. (2001-2011). Anfibios de Parque Nacional Yasuní, Amazonía ecuatoriana. [en línea]. ver. 1.7 (2011). Museo de Zoología, Pontificia Universidad Católica del Ecuador. Quito, Ecuador.

Ron, S. R., Venegas, P. J., Toral, E., Read, Ortiz, D. & Manzano, A. L. (2012) Systematics of the *Osteocephalus buckleyi* species complex (Anura, Hylidae) from Ecuador and Peru. *Zookeys*, 229, 1-52.

Ron, S., & Pramuk, J.B. (1999) A new species of *Osteocephalus* (Anura: Hylidae) from Amazonian Ecuador and Peru. *Herpetologica*, 55:433–446.

Ron, S., Toral, E., Venegas, P. & Barnes, C., (2010) Taxonomic revision and phylogenetic position of *Osteocephalus festae* (Anura, Hylidae) with description of its larva. *ZooKeys*, 70, 67–92.

Savage, J.M. & Heyer, W.R. (1967) Variation and distribution in the tree-frog genus *Phyllomedusa* in Costa Rica, central America. *Beitrage zur Neotropischen Fauna*, 5, 111–131. https://doi.org/10.1080/01650526709360400

Schwarz, G. Estimating the dimension of a model. (1978). *The Annals of Statistics*, 6(2):461–464.

Simmons, M.P. & Kessenich, J. (2020) Divergence and support among slightly suboptimal likelihood gene trees. *Cladistics*, 36, 322–340.

Suárez-Mayorga, A. M. & Lynch, J. D. (2017) Myth and truth on the herpetofauna of Chiribiquete: from the lost world to the last world. *Revista Colombia Amazónica*, 10, 177-190.

Sukumaran, J. & Holder, M.T. (2010) DendroPy: a Python library for phylogenetic computing. *Bioinformatics*, 26: 1569–1571. DOI: 10.1093/bioinformatics/btq228.

Taboada, C., Brunetti, A. E., Lyra, M. L., Fitak, R. R., Soverna, A. F., Ron, S. R., ... & Bari, S. E. (2020) Multiple origins of green coloration in frogs mediated by a novel

biliverdin-binding serpin. *Proceedings of the National Academy of Sciences*, 117(31), 18574-18581.

Trueb, L. & Duellman, W.E. (1970) The systematic status and life history of *Hyla verrucigera* Werner. *Copeia*, 1970, 601. https://doi.org/10.2307/1442303

Trueb, L. & Duellman, W.E. (1971) A synopsis of neotropical hylid frogs, genus *Osteocephalus*. *Occasional papers of the Museum of Natural History*, 1: 1-47.

Trueb, L. (1973) Bones, frogs, and evolution. In Vial JL (Eds) Evolutionary biology of the anurans: contemporary research on major problems. University of Missouri Press, Missouri, 65-132.

Trueb, L. (2015) Osteology. In Duellman WE (Eds) *Marsupial frogs: Gastrotheca and allied genera*. Johns Hopkins University Press, Baltimore, 31–51.

Vaidya, G., Lohman, D.J. & Meier, R. (2011) SequenceMatrix: concatenation software for the fast assembly of multi-gene datasets with character set and codon information. *Cladistics*, 27: 171–180.

Wilkinson, M (1995) Coping with abundant missing entries in phylogenetic inference using parsimony. *Systematic Biology*, 44:501–514.

Supplementary Information

Appendix 1. List of studied specimens for phenotypic characters and their source of data. Available for download **here**

Appendix 2. List of studied specimens for genetic analyses with associated GenBank codes. Available for download **here**

Appendix 3. Raw values of each morphometric variable per specimen. Available for download **here**

Appendix 4. Latitude, longitude, and source of localities mapped in Figure 2. Available for download **here**

TABLES

Table 1. Summary of morphometric variables among adult females (F), males (m), juveniles (J) of *Osteocephalus planiceps* and *O. vilarsi*. N = number of specimens. Minimum and maximum values are followed by average and standard deviation.

	O. planiceps			*O. vilarsi*	
	F (n = 26)	M (n = 19)	J (n = 4)	F (n = 7)	M (n = 9)
SVL	50.8–80.7 (66.8 ± 9.1)	48.9–67.6 (57.3 ± 5.2)	33.8–46.8 (40.5 ± 5.7)	56.0–73.8 (63.0 ± 6.4)	50.7–61.5 (56.2 ± 3.8)
HL	16.9–28.4 (23.4 ± 3.3)	17.5–23.3 (23.3 ± 1.6)	12.5–16.3 (14.4 ± 2.1)	19.2–25.4 (21.8 ± 2.3)	17.8–20.0 (19.0 ± 0.8)
HW	16.4–26.6 (21.7 ± 2.9)	15.7–21.8 (18.9 ± 1.5)	11.2–14.9 (13.6 ± 1.6)	18.3–24.3 (20.6 ± 2.1)	17.1–19.6 (18.4 ± 1.0)
IOD	5.9–10.6 (8.1 ± 1.4)	5.3–8.3 (6.6 ± 0.8)	4.1–5.8 (4.9 ± 0.9)	6.1–10.4 (7.4 ± 1.5)	5.5–7.7 (6.5 ± 0.7)
ED	4.4–7.8 (5.8 ± 0.9)	3.8–6.4 (5.1 ± 0.6)	3.4–4.5 (4.1 ± 0.5)	5.3–6.6 (5.9± 0.5)	4.4–5.3 (4.9 ± 0.3)
END	7.7–13.4 (10.4 ± 1.7)	7.5–10.3 (8.8 ± 0.7)	5.2–7.4 (6.2 ± 1.0)	8.2–11.2 (9.5 ± 1.0)	7.4–8.9 (8.2 ± 0.5)
TD	3.4–6.7 (5.1 ± 0.9)	4.2–5.6 (4.7 ± 0.4)	2.4–3.8 (3.2 ± 0.6)	4.3–6.3 (5.0 ± 0.7)	4.0–5.0 (4.5 ± 0.4)
VTD	3.1–6.0 (4.3 ± 0.7)	3.3–5.0 (4.0 ± 0.4)	2.4–3.0 (2.8 ± 0.3)	3.7–4.9 (4.3 ± 0.5)	3.4–4.1 (3.8 ± 0.2)
IND	3.5–5.5 (4.5 ± 0.6)	3.2–4.6 (4.0 ± 0.4)	2.8–3.6 (3.2 ± 0.3)	4.2–5.7 (4.6 ± 0.5)	3.6– 4.6 (4.1 0.3)
NSD	1.8–3.6 (2.6 ± 0.5)	1.8–2.8 (2.3 ± 0.3)	1.5–2.1 (1.8 ± 0.3)	2.3–3.1 (2.6 ± 0.3)	2.0–2.8 (2.5 ± 0.3)
THL	27.7–46.4 (35.8 ± 5.5)	25.5–36.4 (30.9 ± 3.1)	18.1–25.4 (21.6 ± 3.2)	29.7–41.7 (34.3 ± 4.0)	25.1–33.1 (29.2 ± 2.7)
TL	29.9–48.9 (38.6 ± 5.5)	28.5–37.5 (32.9 ± 2.8)	18.9–26.9 (22.9 ± 3.5)	31.5–43.2 (36.3 ± 3.8)	28.0–35.3 (31.5 ± 2.5)
FL	21.8–36.9 (28.3 ± 4.3)	20.2–28.4 (24.1 ± 2.3)	13.4–19.2 (16.2 ± 2.6)	23.5–33.6 (27.1± 3.5)	20.9–26.1 (23.5 ± 1.8)
4F	2.0–4.2 (3.1 ± 0.5)	2.1–3.2 (2.8 ± 0.3)	1.6–2.2 (1.8 ± 0.3)	2.5–3.8 (3.0 ± 0.5)	2.6–3.3 (2.8 ± 0.2)
HAL	15.3–26.3 (20.9 ± 3.1)	14.9–21.0 (17.8 ± 1.6)	10.3–14.6 (11.8 ± 2.1)	17.3–24.0 (20.2 ± 2.5)	15.9–19.9 (17.5 ± 1.3)
3F	2.6–5.0 (3.7 ± 0.7)	2.3–3.8 (3.2 ± 0.4)	1.7–2.3 (2.0 ± 0.2)	3.0–4.9 (3.6 ± 0.7)	3.0–3.3 (3.1 ± 0.1)

Table 2. Loadings of morphometric variables of a PCA of the raw measurements and the residuals of a linear correlation with SVL. The highest and lowest loading values are in bold face.

Raw morphometrics			Residuals with SVL		
Variable	PC1	PC2	Variable	PC1	PC2
SVL	**-0.68**	**0.49**	—	**—**	—
TL	-0.39	**-0.45**	TL	-0.22	-0.28
THL	-0.36	**-0.52**	THL	**0.02**	-0.20
FOOT	-0.29	-0.32	FOOT	-0.02	-0.01
HL	-0.24	0.30	HL	**-0.64**	-0.22
HW	-0.22	0.25	HW	**-0.61**	**0.45**
HAND	-0.21	-0.10	HAND	-0.41	-0.10
END	-0.10	0.04	END	-0.03	-0.16
IOD	-0.08	-0.05	IOD	-0.01	-0.08
ED	-0.06	0.13	ED	-0.06	-0.08
TD	-0.05	0.05	TD	-0.04	**-0.50**
IND	-0.05	0.04	IND	0.00	0.01
TH	-0.05	0.07	TH	-0.02	-0.19
X3F	-0.04	0.01	X3F	-0.01	-0.03
X4F	-0.03	0.02	X4F	0.00	-0.15
NSD	-0.03	0.03	NSD	**0.02**	**-0.52**
Eigenvalue	91.4	1.6	Eigenvalue	1.9	1.0
Variance(%)	92.4	1.6	Variance(%)	24.9	12.7
Accumulative variance(%)	92.4	94.0	Accumulative variance(%)	24.9	37.5

Table 3. Models of nucleotide evolution and dataset partitions used in maximum likelihood phylogenetic analysis. Numbers after an "-" indicate codon position for protein coding genes.

Model	Partitions
TIM2+F+R3	12S, 16S, ND1-1, CYTB-2, tRNA-Ile, tRNA-Gln, tRNA-Leu, tRNA-Val
TIM2e+R2	COI-1, POMC-1, ROH-1, RAG12, TNS3-2, TYR-1
HKY+F+R2	COI-2, ND1-2, ROH-3, CYTB-3
TN+F+I+G4	COI-3, ND1-3, CYTB-1
TPM3+F+I	POMC-2, POMC-3, ROH-2, RAG1-1, RAG1-3, SIAH-1, SIAH-2, SIAH-3, TNS3-1, TNS3-3, TYR-2, TYR-3

Table 4. Intraspecific (diagonal) and interspecific (below the diagonal) uncorrected genetic p-distances among specimens of the *Osteocephalus planiceps* species group inferred from a DNA sequences of fragments of the mitochondrial genes 16S and COI (see main text for details). N = number of specimens per species. Minimum and maximum values are followed by average and standard deviation.

16S	**1**	**2**	**3**	**4**	**5**	**6**
(1) *O. castaneicola* n = 8	0.0–1.0 (0.7 ± 0.4)					
(2) *O. deridens* n = 4	0.0–6.3 (5.3 ± 1.3)	0.0–1.5 (1.0 ± 0.8)				
(3) *O. fuscifacies* n = 4	4.3–6.1 (5.4 ± 0.4)	4.9–6.3 (5.7 ± 0.4)	0.3–1.5 (1.1± 0.4)			
(4) *O. leoniae* n = 4	4.8–6.9 (6.1 ± 0.7)	5.7–7.8 (6.9 ± 0.8)	5.1–7.5 (6.5 ± 0.8)	0.0–4.6 (3.5 ± 1.8)		
(5) *O. planiceps* n = 32	1.8–4.0 (3.1 ± 0.4)	3.4–5.4 (4.0 ± 0.5)	3.1–5.7 (4.5 ± 0.5)	3.1–6.5 (5.3 ± 0.7)	0.0–3.4 (1.3 ± 0.9)	
(6) *O. vilarsi* n = 15	3.7–4.8 (4.4 ± 0.3)	4.5–5.1 (4.6 ± 0.2)	4.5–5.7 (5.1 ± 0.4)	5.0–7.5 (6.3 ± 0.8)	2.1–4.5 (2.9 ± 0.6)	0.0–2.9 (0.8 ± 0.8)
COI	**1**	**2**	**3**	**4**	**5**	**6**
(1) *O. castaneicola* n = 3	0.8–1.4 (1.1 ± 0.3)					
(2) *O. deridens* n = 3	9.9–11.5 (10.6± 0.7)	0.0–4.8 (3.2 ± 2.8)				
(3) *O. fuscifacies* n = 2	10.8–11.7 (11.7± 0.4)	6.3–10.6 (7.7 ± 2.2)	0.0–0.0 (0.0± 0.0)			
(4) *O. leoniae* n = 2	10.0–10.8 (10.3 ± 0.4)	9.2–9.4 (9.3 ± 0.1)	9.2–9.2 (9.2 ± 0.0)	0.0–0.0 (0.0± 0.0)		
(5) *O. planiceps* n = 15	6.3–17.5 (8.5 ± 3.3)	9.2–17.9 (11.1 ± 2.4)	8.6–16.3 (10.4 ± 2.4)	8.5–17.3 (10.3 ± 2.8)	0.0–16.7 (6.4 ± 5.4)	
(6) *O. vilarsi* n = 3	8.2–10.1 (9.0± 0.6)	9.6–12.0 (10.7± 0.9)	9.7–10.3 (9.9 ± 0.3)	10.1–12.2 (11. ± 1.0)	6.3–15.9 (8.9 ± 2.5)	0.0–5.5 (2.7 ± 2.7)

Table 5. Bone color variation according to sex and ontogeny across three localities in Loreto, Peru. Numbers refer to number of specimens.

	White			Green		
	Female	Male	Juvenile	Female	Male	Juvenile
EBJAA	1	0	0	8	3	2
CIJH	3	4	0	4	5	1
Frontera	4	7	1	1	0	1

FIGURE

Figure 1. Holotype of *Osteocephalus planiceps* (ANSP 11399), an adult male (SVL = 58.5 mm) from Nauta, Loreto, Peru. Note the white subocular mark and the elevated lateral edges of the frontoparietals. Scale bar = 10 mm. Photographs by Ned Gilmore.

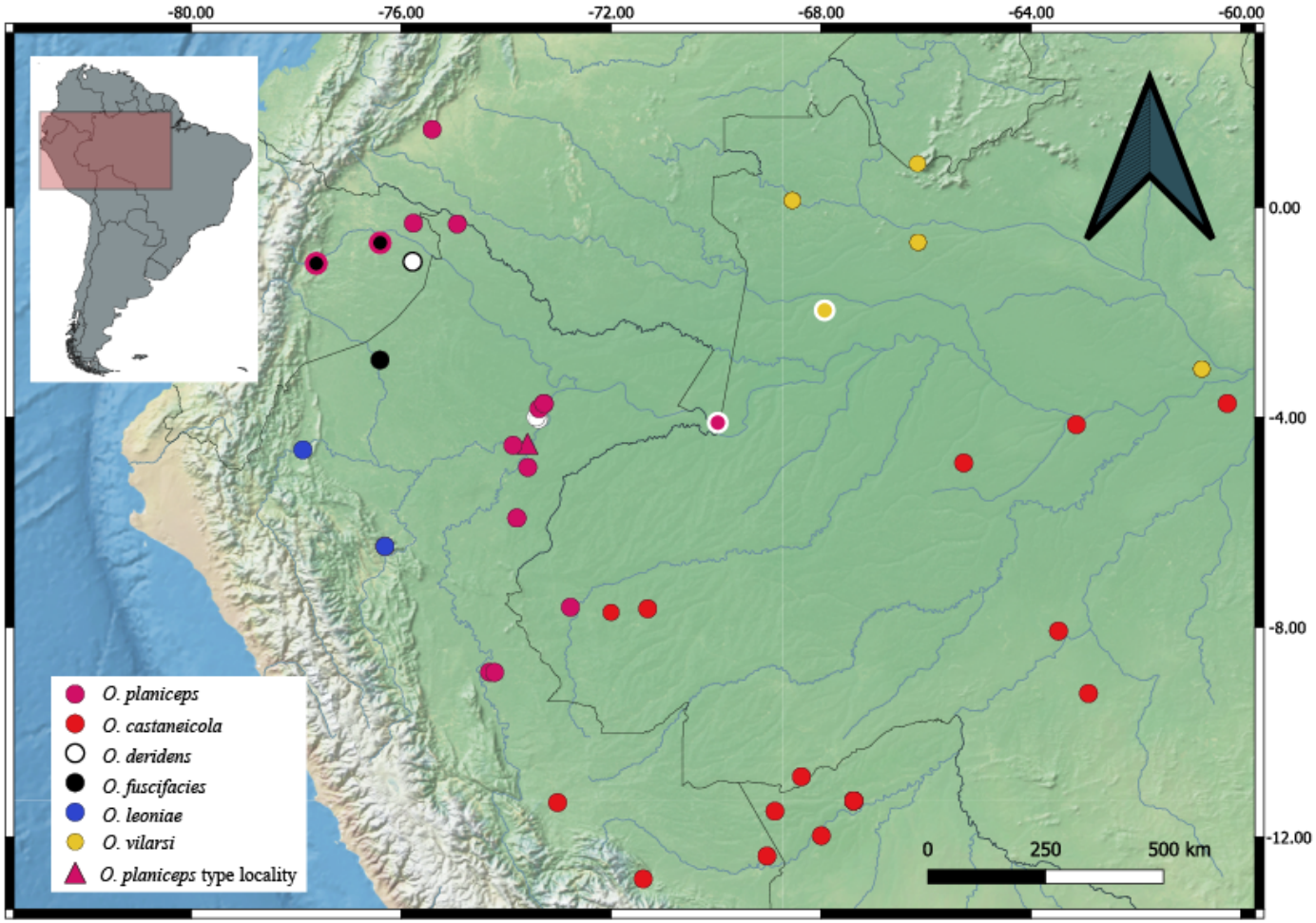

Figure 2. Map of western Amazonia with dots indicating localities of species of the *Osteocephalus planiceps* species group. Dots with two colors indicate cases of sympatry. We only represent localities based on identification confirmed by analysis of DNA sequences except for *O. castaneicola*, which include additional localities based on the recent review by Melo-Sampaio *et al*. (2021).

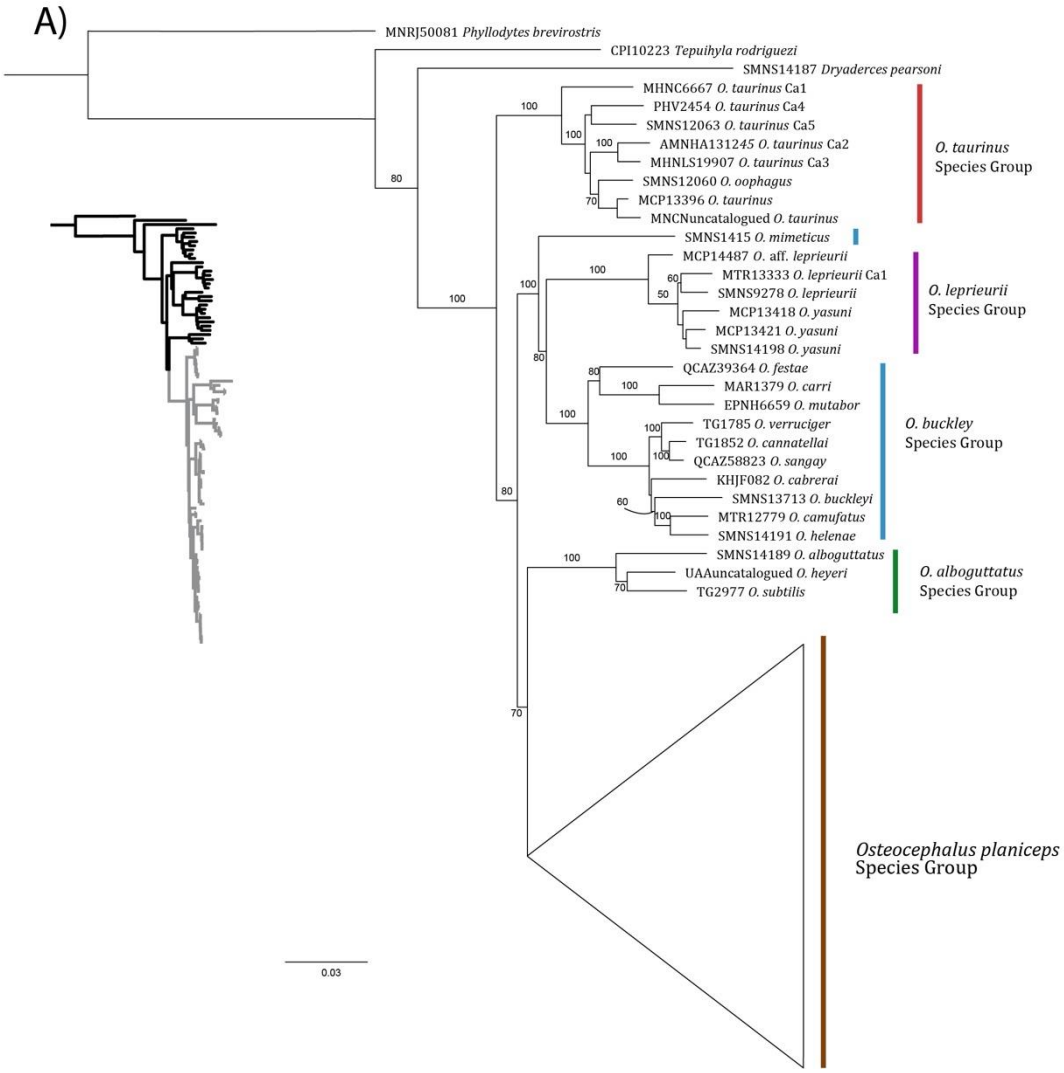
A)
MNRJ50081 Phyllodytes brevirostris
CPI10223 Tepuihyla rodriguezi
SMNS14187 Dryaderces pearsoni
MHNC6667 O. taurinus Ca1
PHV2454 O. taurinus Ca4
SMNS12063 O. taurinus Ca5
AMNHA131245 O. taurinus Ca2
MHNLS19907 O. taurinus Ca3
SMNS12060 O. oophagus
MCP13396 O. taurinus
MNCNuncatalogued O. taurinus
O. taurinus Species Group
SMNS1415 O. mimeticus
MCP14487 O. aff. leprieurii
MTR13333 O. leprieurii Ca1
SMNS9278 O. leprieurii
MCP13418 O. yasuni
MCP13421 O. yasuni
SMNS14198 O. yasuni
O. leprieurii Species Group
QCAZ39364 O. festae
MAR1379 O. carri
EPNH6659 O. mutabor
TG1785 O. verruciger
TG1852 O. cannatellai
QCAZ58823 O. sangay
KHJF082 O. cabrerai
SMNS13713 O. buckleyi
MTR12779 O. camufatus
SMNS14191 O. helenae
O. buckley Species Group
SMNS14189 O. alboguttatus
UAAuncatalogued O. heyeri
TG2977 O. subtilis
O. alboguttatus Species Group
Osteocephalus planiceps Species Group
0.03

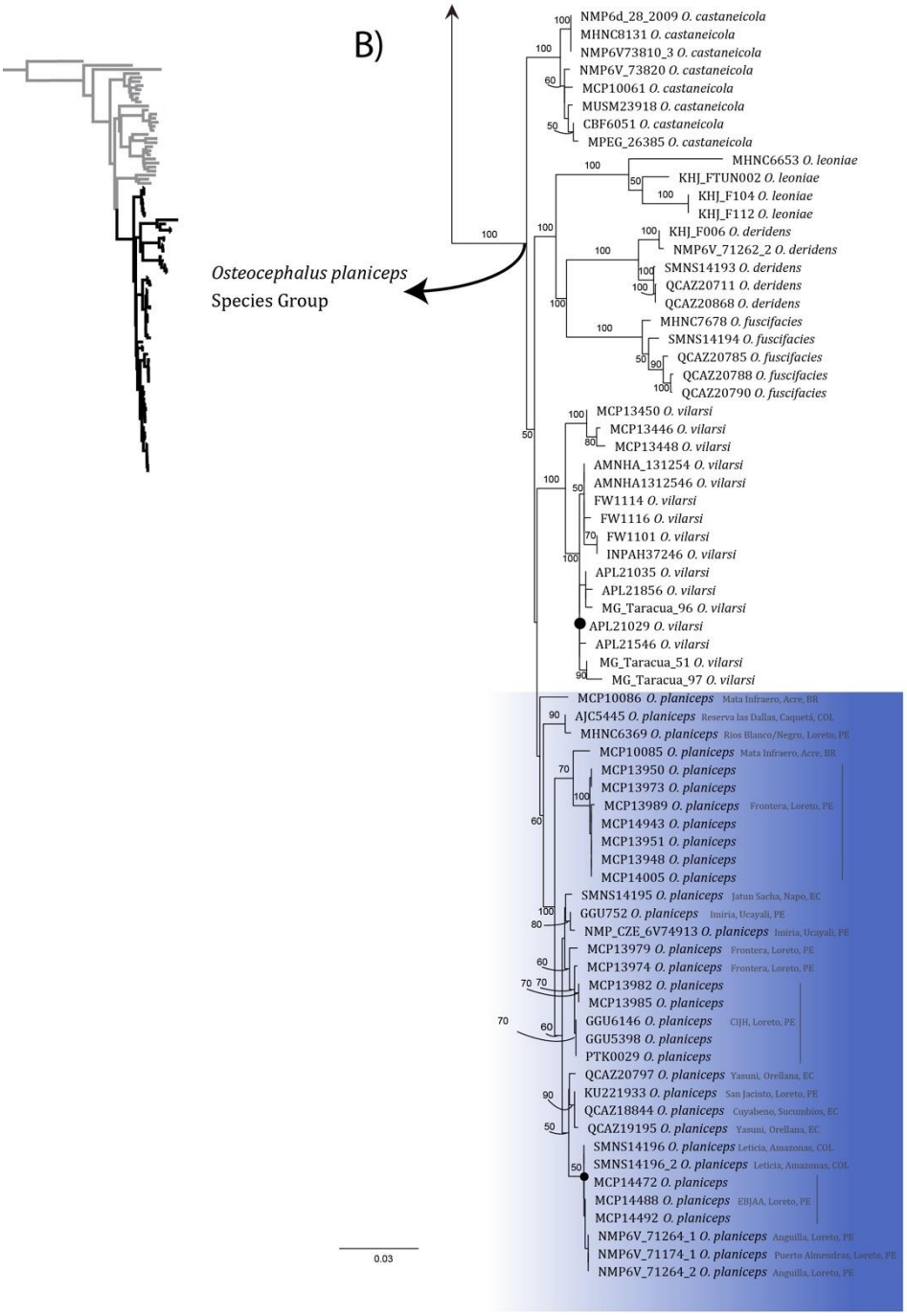

Figure 3. Phylogenetic relationships of *Osteocephalus* (log likelihood = -39153.5227) inferred from a maximum likelihood analysis of 7667 bp of mitochondrial and nuclear genes and considering indels as unknown nucleotides. Numbers on branches are bootstrap frequencies (percentage) of 1000 pseudoreplicates. Only bootstrap values above 50 are shown. (A) Relationships among outgroups and *Osteocephalus* species outside the *O. planiceps* species groups. (B) Relationships among species of the *O. planiceps* species groups, with specimens of *O. planiceps* highlighted in blue. A skeletal topology, with the magnified section marked in black, is shown on the left side.

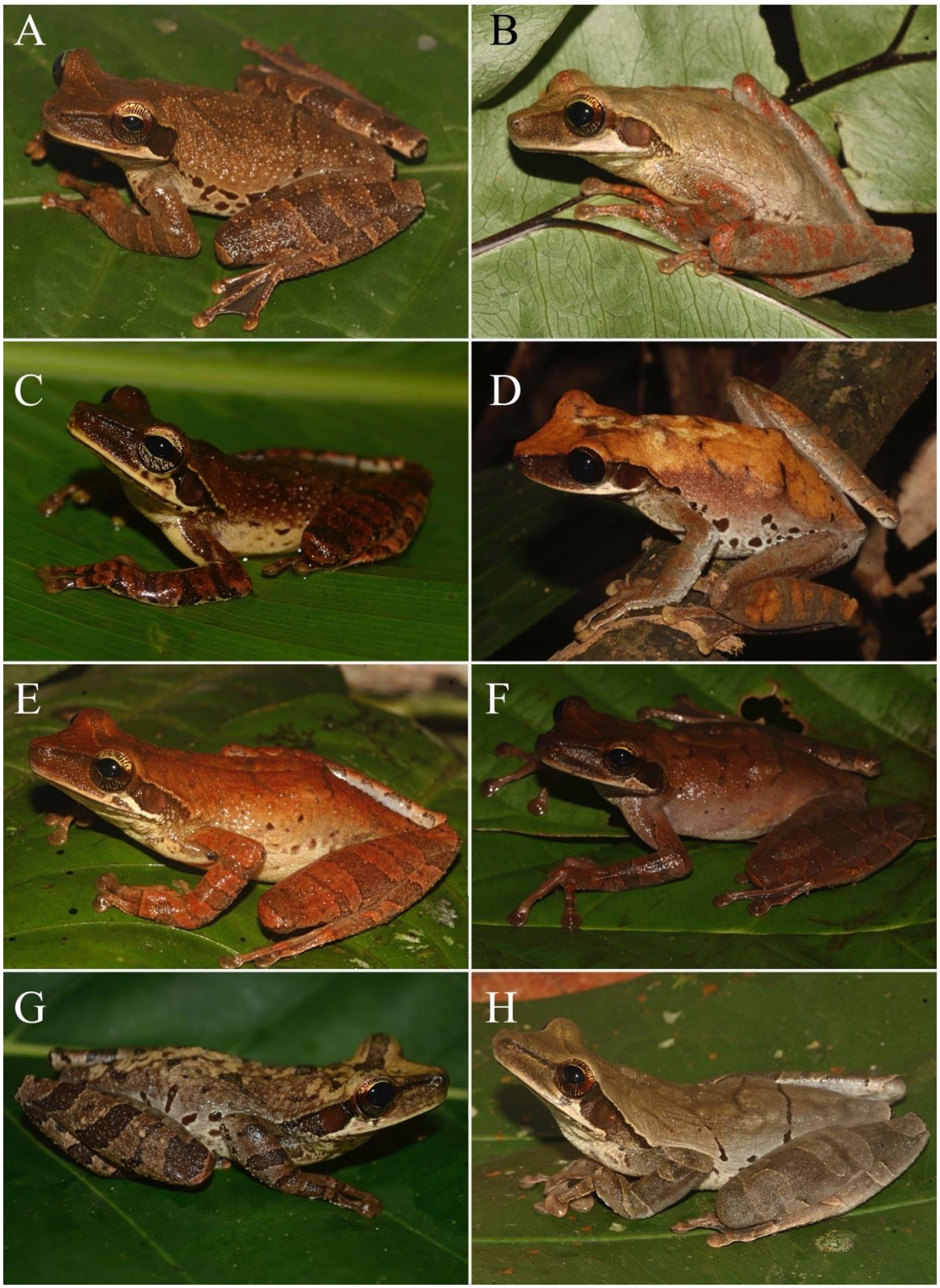

Figure 4. Adult specimens of *Osteocephalus planiceps* from Loreto, Peru, in life. (A) MCP 14492, male from EBJAA. (B) GGU 5509, female from CIJH. (C) MCP 13974, male from Frontera. (D) GGU 5673, female from EBJAA. (E) MCP 14480, male from CIJH. (F) GGU 5398, female from CIJH. (G) MCP 13985, male from CIJH. (H) MCP 14490, female from EBJAA. Photographs by GG-U and PT.

Figure 5. Lateral view of the head of a live adult male **(**MCP 14484) of *Osteocephalus planiceps* from Frontera, Loreto, Peru. Photograph by GG-U.

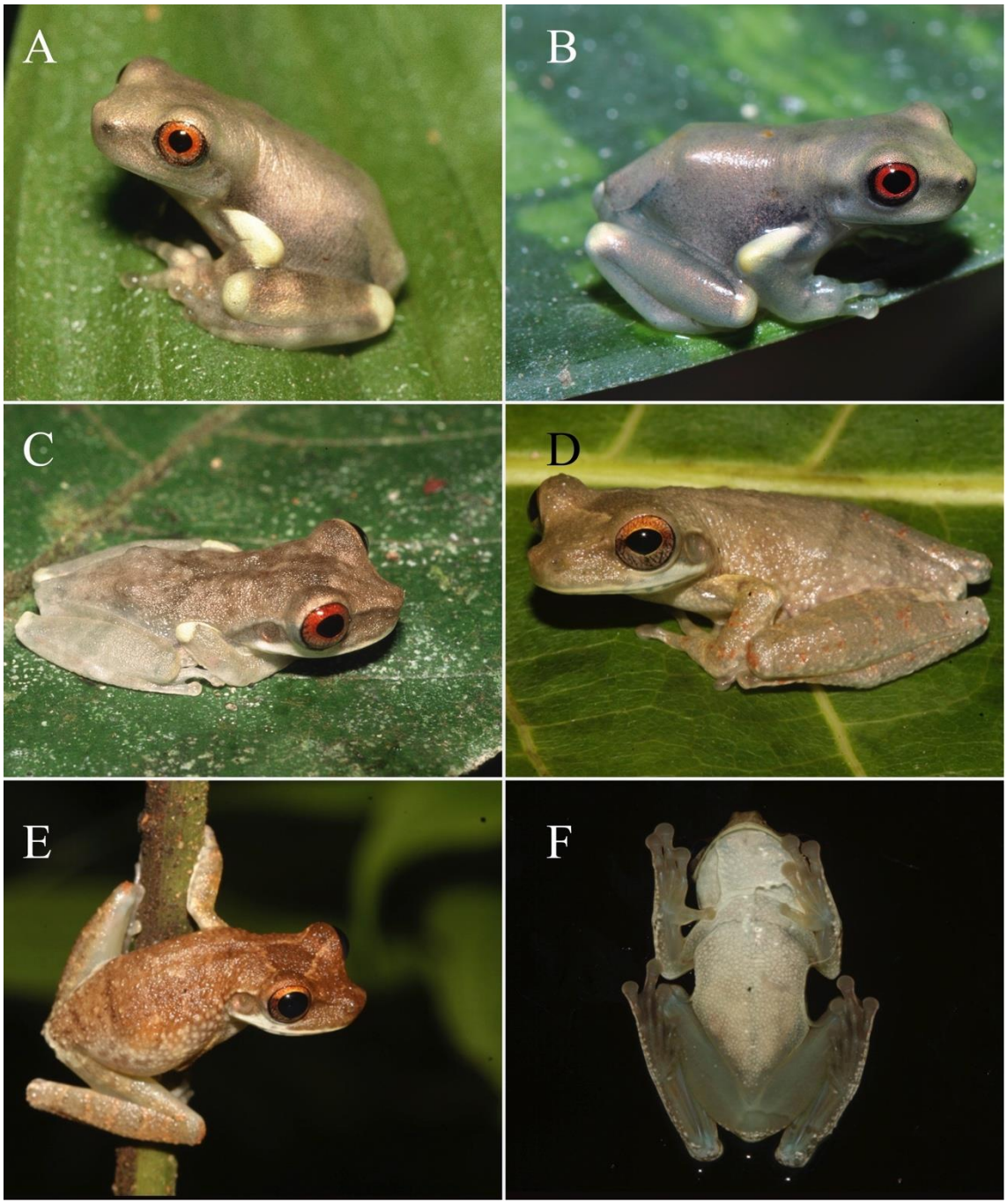

Figure 6. Live non-adult specimens of *Osteocephalus planiceps*. Recent metamorphs, (A) KHJ 286 from Jatun-Sacha, Napo, Ecuador, and (B) KHJ 2099 from Quebrada Negra, Loreto, Peru. (C) A more developed metamorph, KHJ S2-079, from Leticia, Amazonas, Colombia. (D–F) a subadult (MCP 5517) from CIJH, Loreto, Peru, note the darker coloration of the specimen *in natura*. Photographs by KHJ (A–C) and GG-U (D–F).

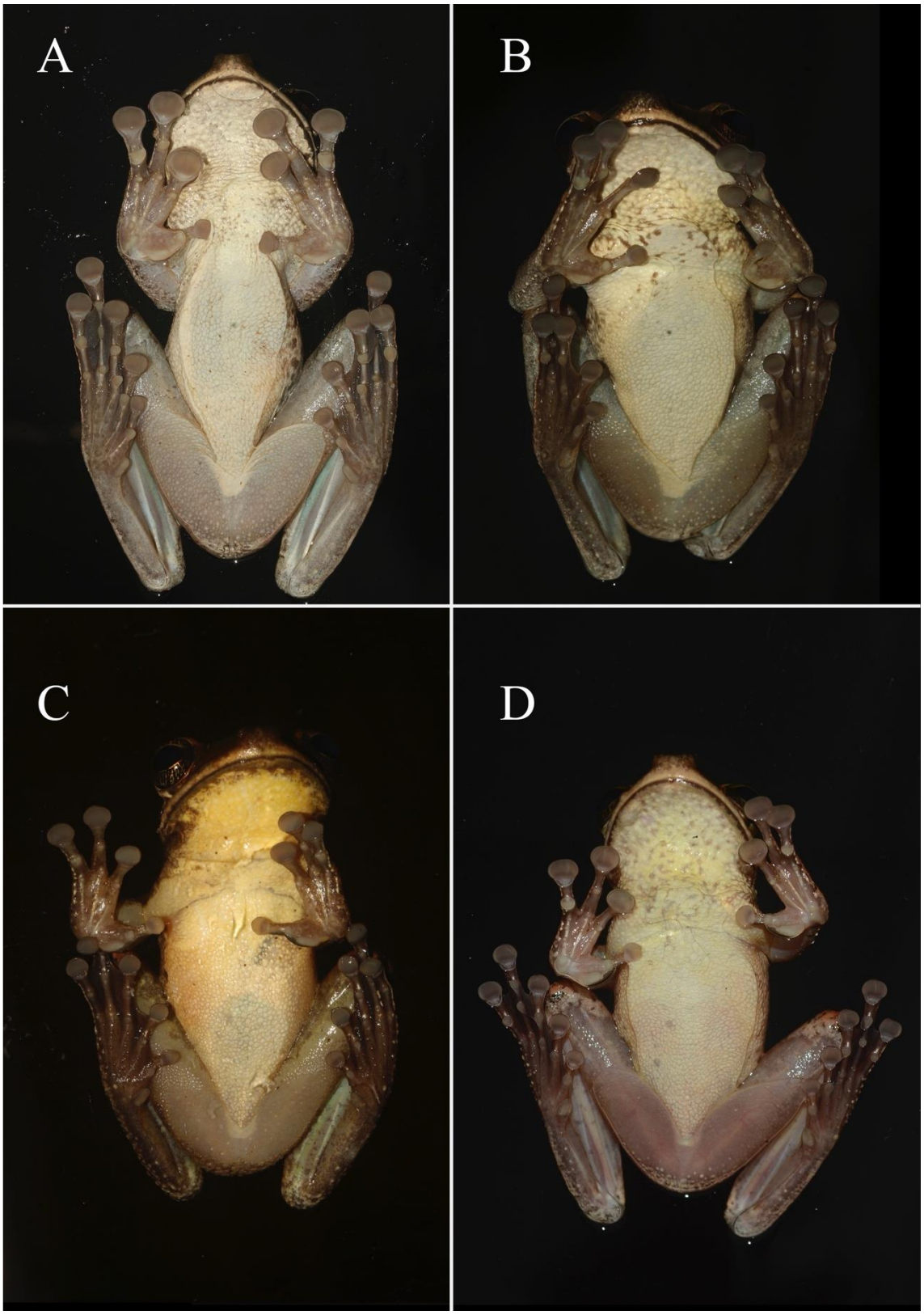

Figure 7. Ventral view of live adults of *Osteocephalus planiceps* from Loreto, Peru. (A) MCP 14490, female, from EBJAA. (B) GGU 5702, female, from EBJAA. (C) MCP 14484, male, from CIJH. (D) MCP 13950, male, from Frontera. Photographs by GG-U and PT.

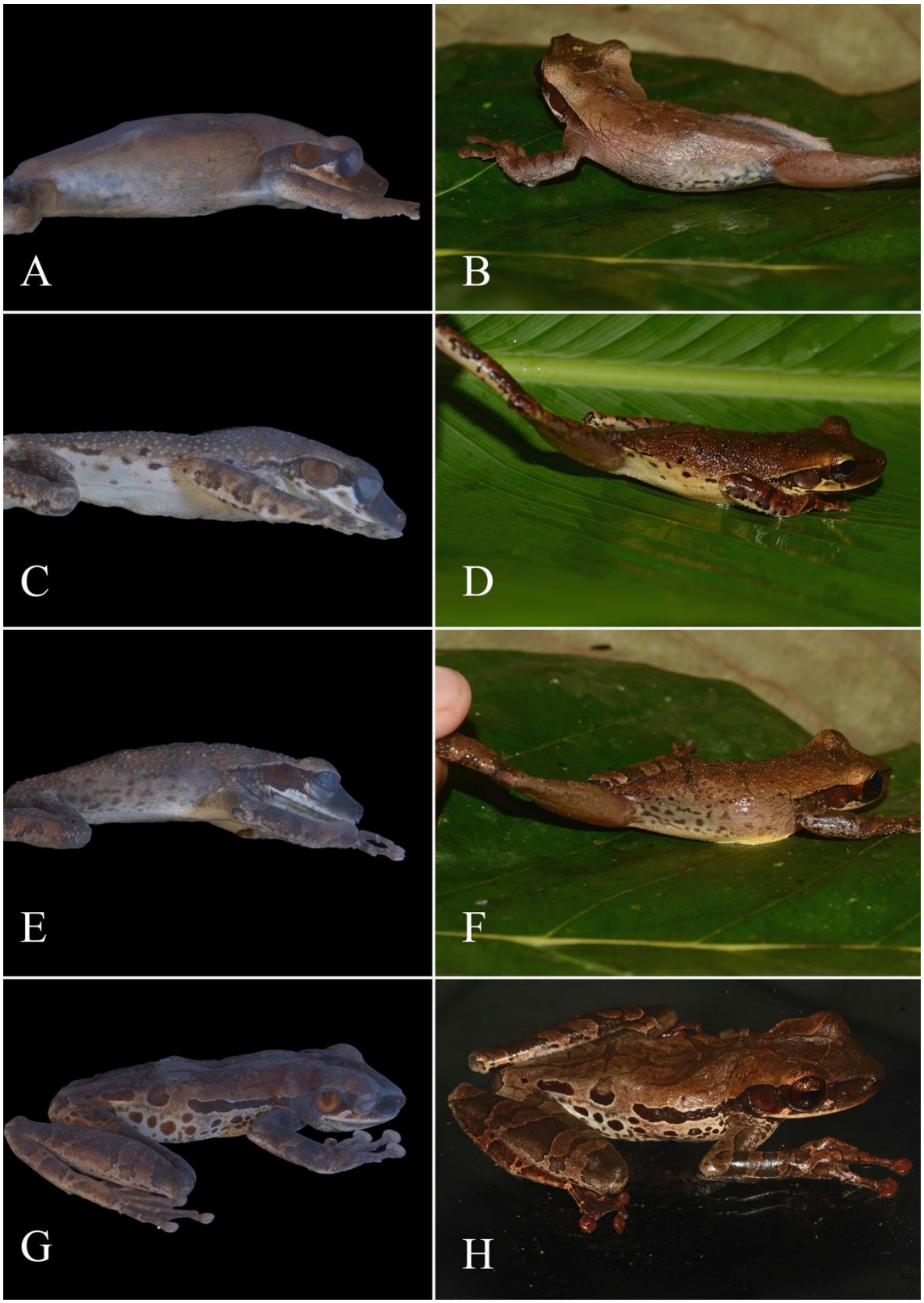

Figure 8. Lateral view of flanks of adult *Osteocephalus planiceps* from Loreto, Peru, in preservative and life . (A, B) MCP 14001, female, from CIJH. (C, D) MCP 13947, male, from Frontera. (E, F) MCP 13999, male, from CIJH. (G, H) GGU 5841, female, from EBJAA. Photographs by GG-U and PT.

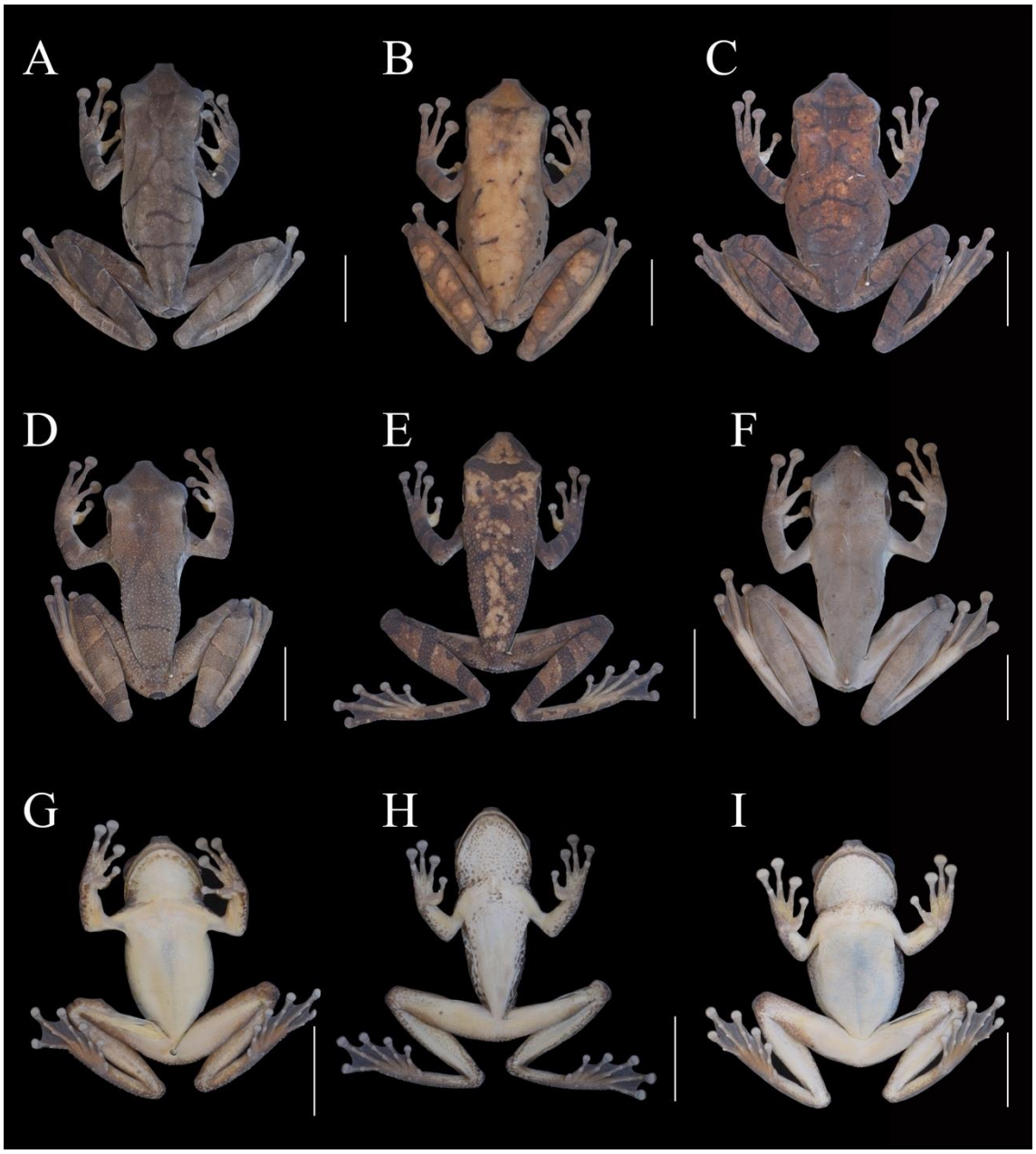

Figure 9. Adult preserved specimens of *Osteocephalus planiceps* from Loreto, Peru, showing variation in dorsal and ventral coloration. (A) MCP 14490, female, from EBJAA. (B) GGU 5673, female, from EBJAA. (C, I) MCP 14012, female, from Frontera. (D) MCP 14492, male, from EBJAA. (E, H) MCP 13985, male, from CIJH. (F) GGU 5714, female, from EBJAA. (G) MCP 14484, male, from CIJH. Scale bar = 1 cm. Photographs by PT.

Figure 10. Ventral view of the right hand and foot of *Osteocephalus planiceps* MCP 14481, adult female. Scale bar = 1 cm. Photograph by PT.

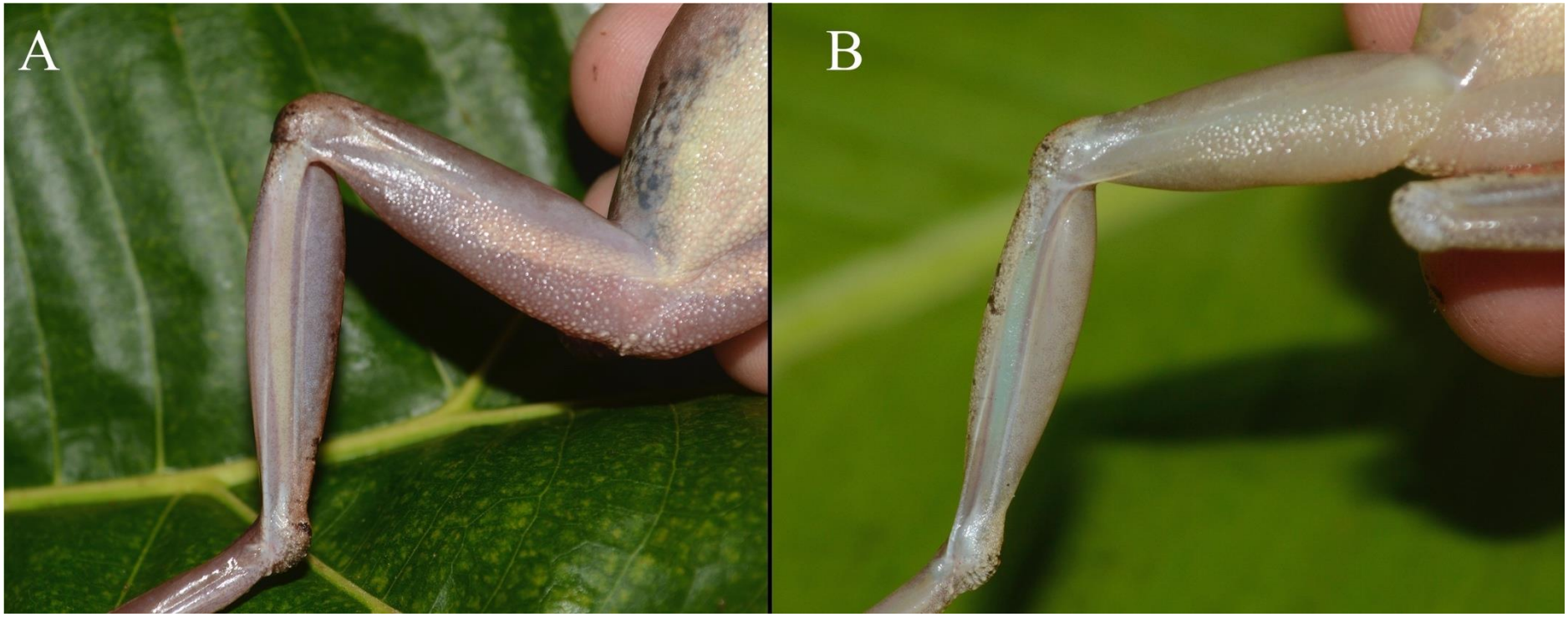

Figure 11. Ventral view of hindlimbs of two specimens of *Osteocephalus planiceps* from Loreto, Peru, showing bone color variation in tibiofibular and femur bones. (A) MCP 14005, female, from Frontera. (B) MCP13980, juvenile, from Frontera. Photographs by PT.

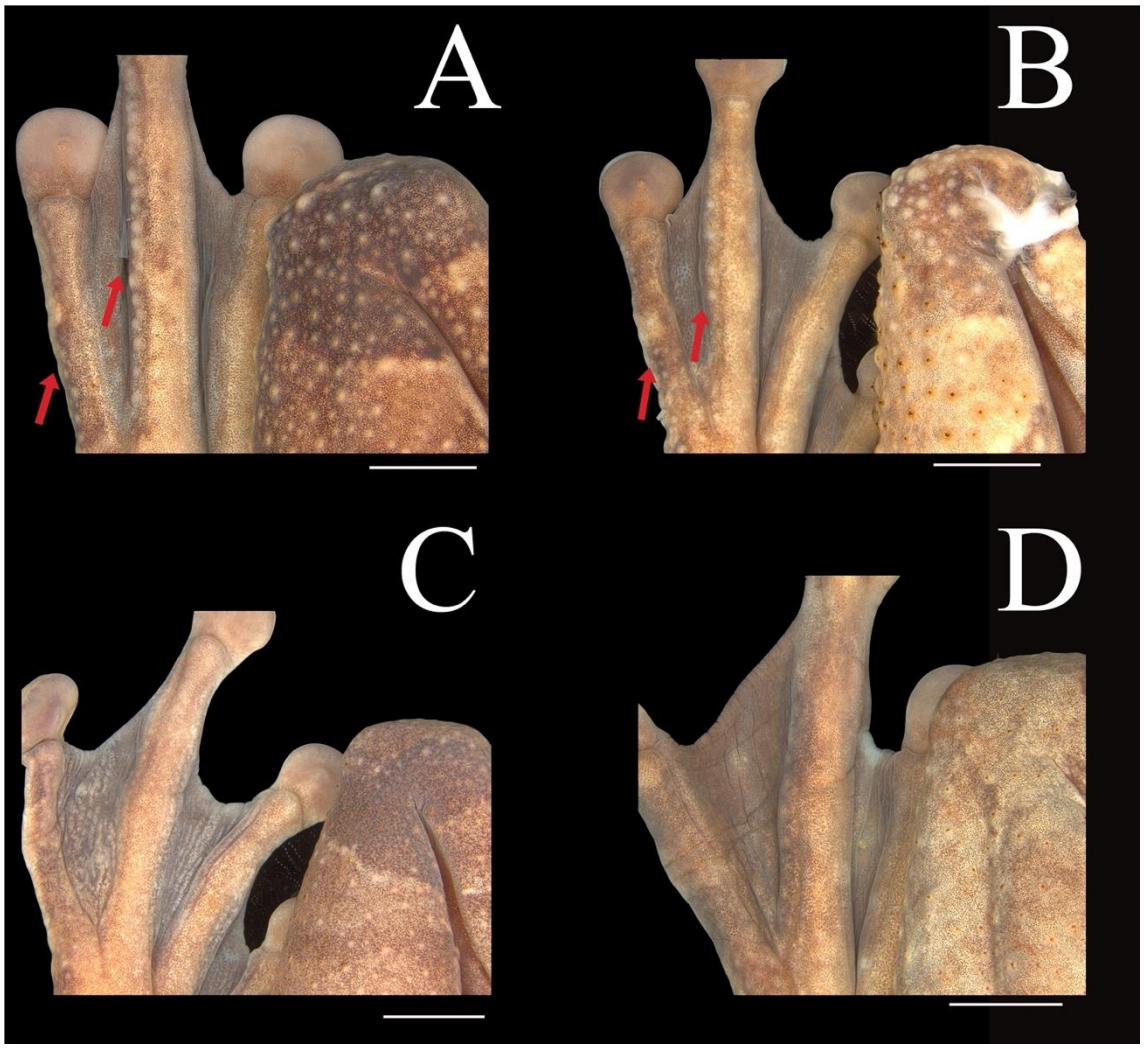

Figure 12. Dorsal view of the left foot of four species of *Osteocephalus*. (A) *O. planiceps* MCP 14492. (B) *O. vilarsi* MCP 13413. (C) *O. castaneicola* MCP 10062. (D) *O. taurinus* MCP 13396. Arrows point to a row of distal tubercles. Scale bar = 3 mm.

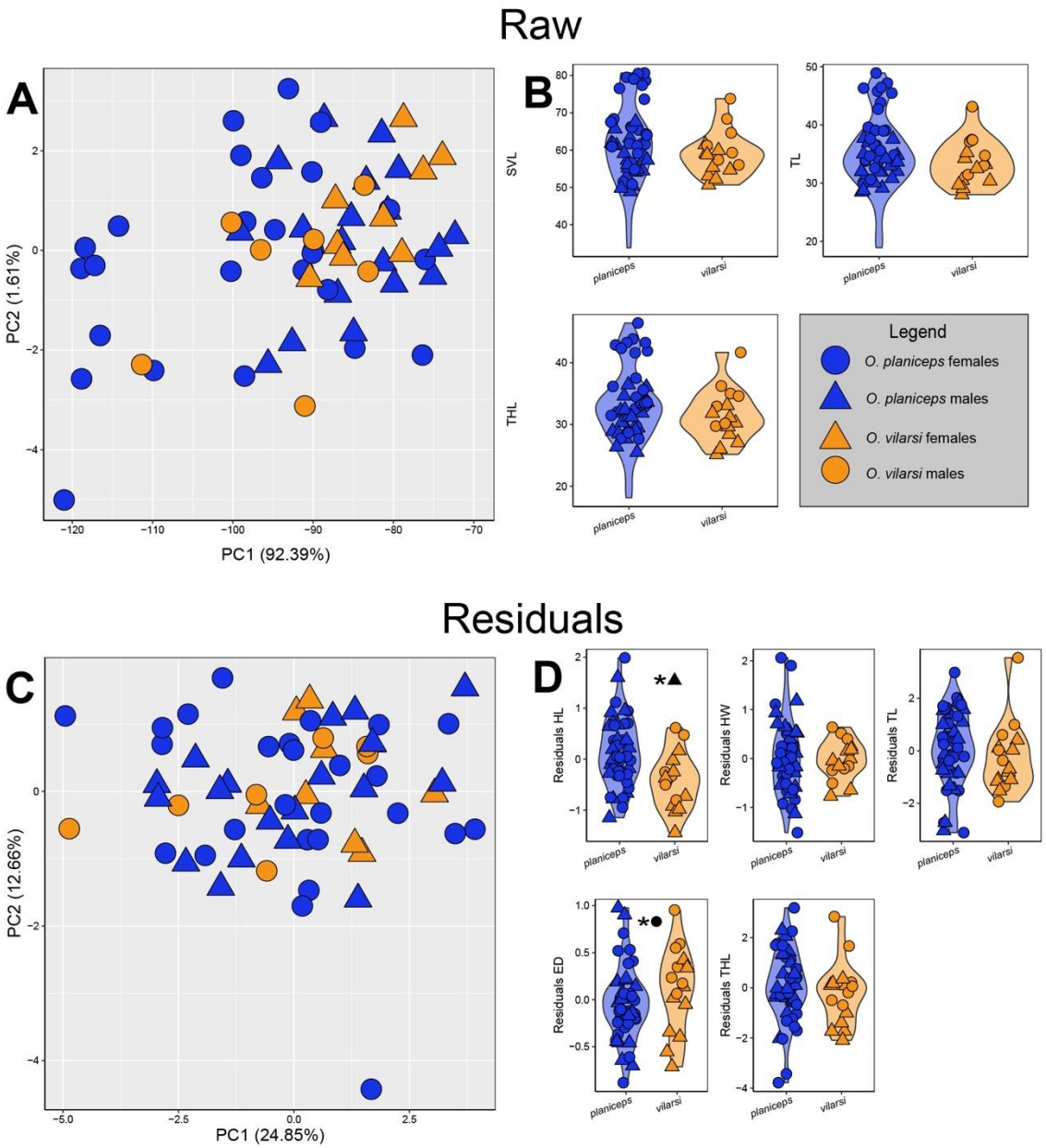

Figure 13. Principal component analysis plot of the raw measurements (A) and the residuals of a correlation with SVL (C) of adult males and females of *Osteocephalus planiceps* and *O. vilarsi*. The variance explained by each axe is in parentheses. Violin plots of the morphometric variables with the higher loadings on the PCAs based on the raw measurements (B) and the residuals with SVL (D). An asterisk (*) denotes statistically significant differences ($p < 0.05$) when comparing the average values by sex and variable of each species.

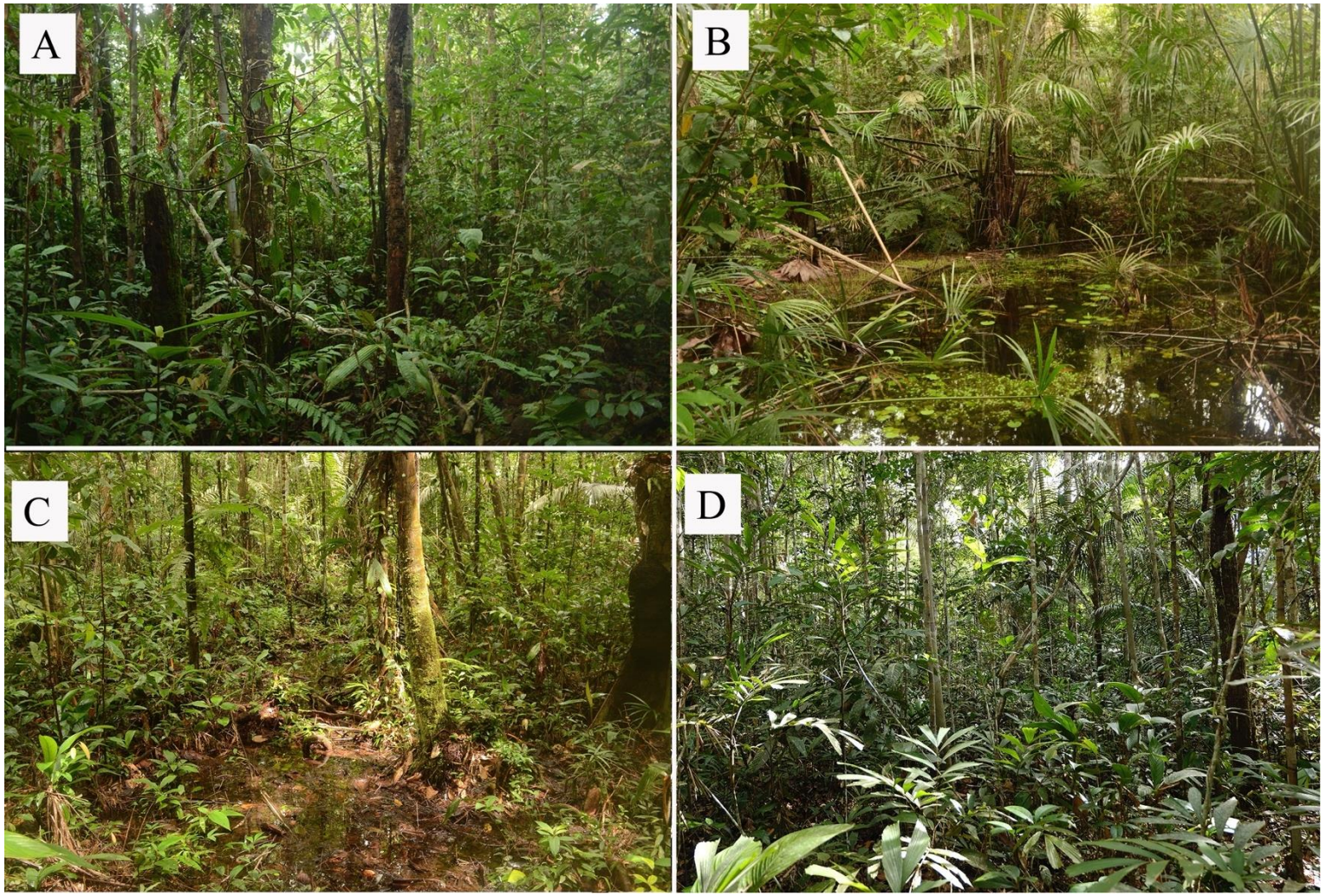

Figure 14. Habitats of *Osteocephalus planiceps* in two localities of Loreto, Peru. (A) *terra-firme* forest in CIJH. (B) flooded forest floor in CIJH (C) temporary pond in CIJH. (D) white-sand forest in Frontera.

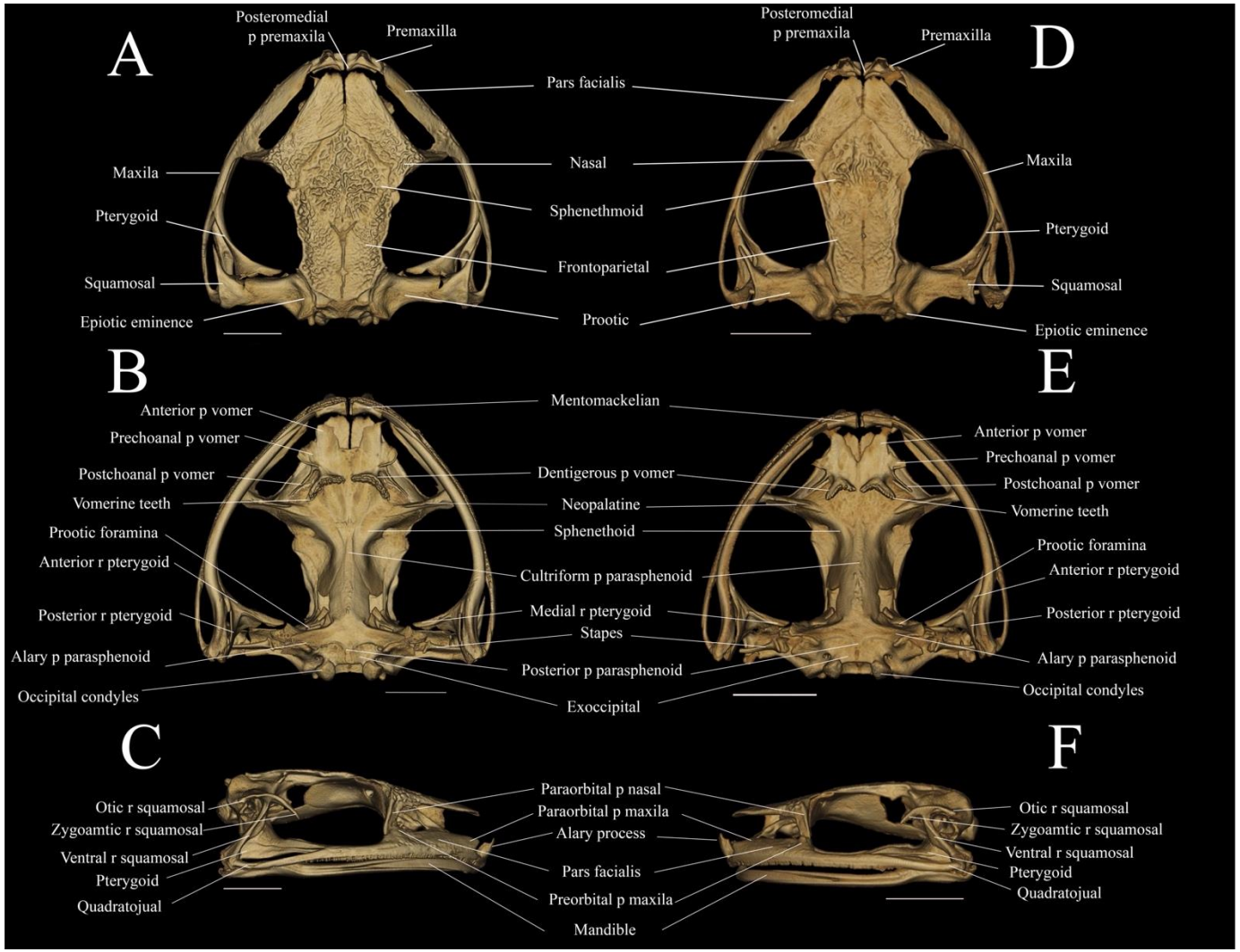

Figure 15. Skull of *Osteocephalus planiceps* and *O. vilarsi* in dorsal (top), ventral (middle), and lateral (bottom) views. (A–C) *O. planiceps* MCP 14992 and (D–F) *O. vilarsi* INPAH 40468. Scale bar = 5 mm.

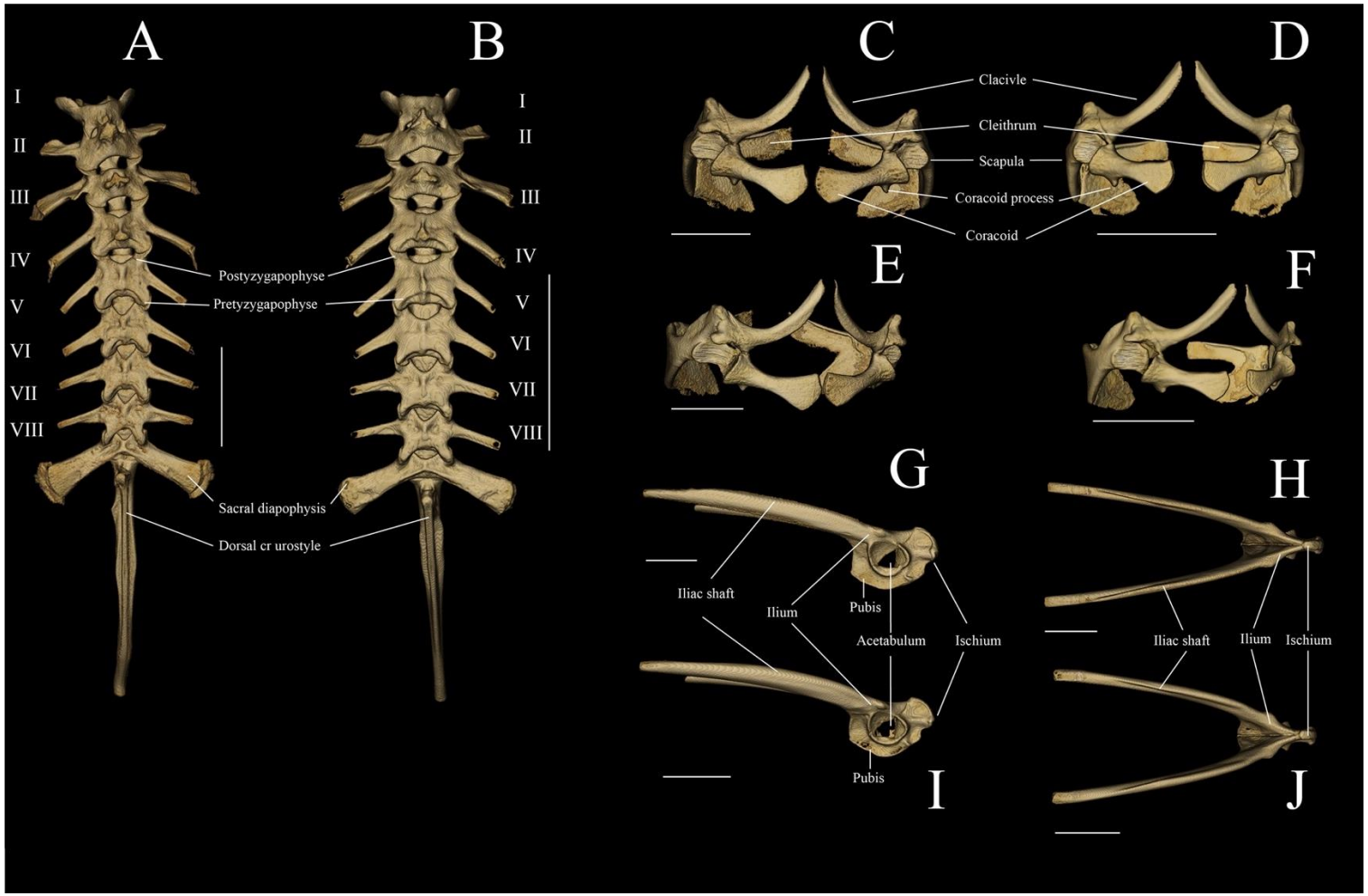

Figure 16. Axial (left half) and girdle (right half) calcified elements of the skeleton of *Osteocephalus planiceps* MCP 14990 (A, C, E, G, I) and *O. vilarsi* INPAH 40470 (B, D, F, H, J).
Scale bar = 10 mm (AB) and 5 mm (C–J).

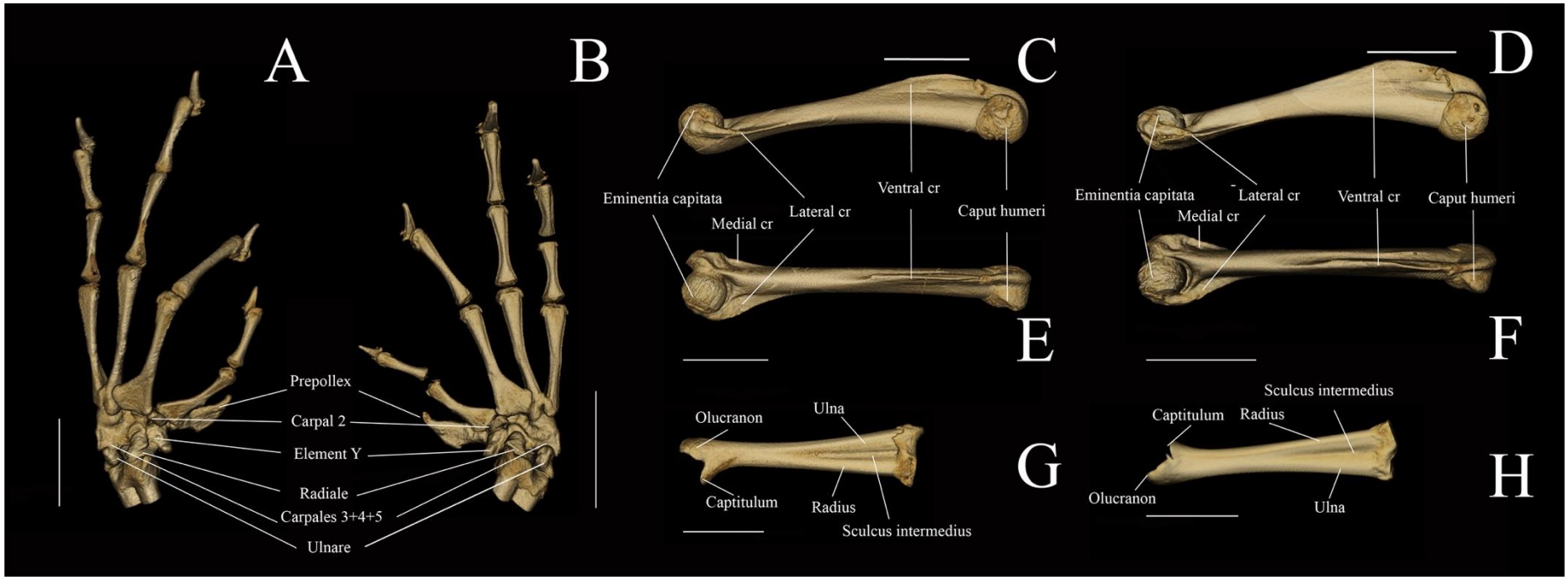

Figure 17. Calcified elements of the forelimb skeleton of *Osteocephalus planiceps* MCP 14990 (A, C, E, G) and *O. vilarsi* INPAH 40470 (B, D, F, H). Scale bar = 5 mm.

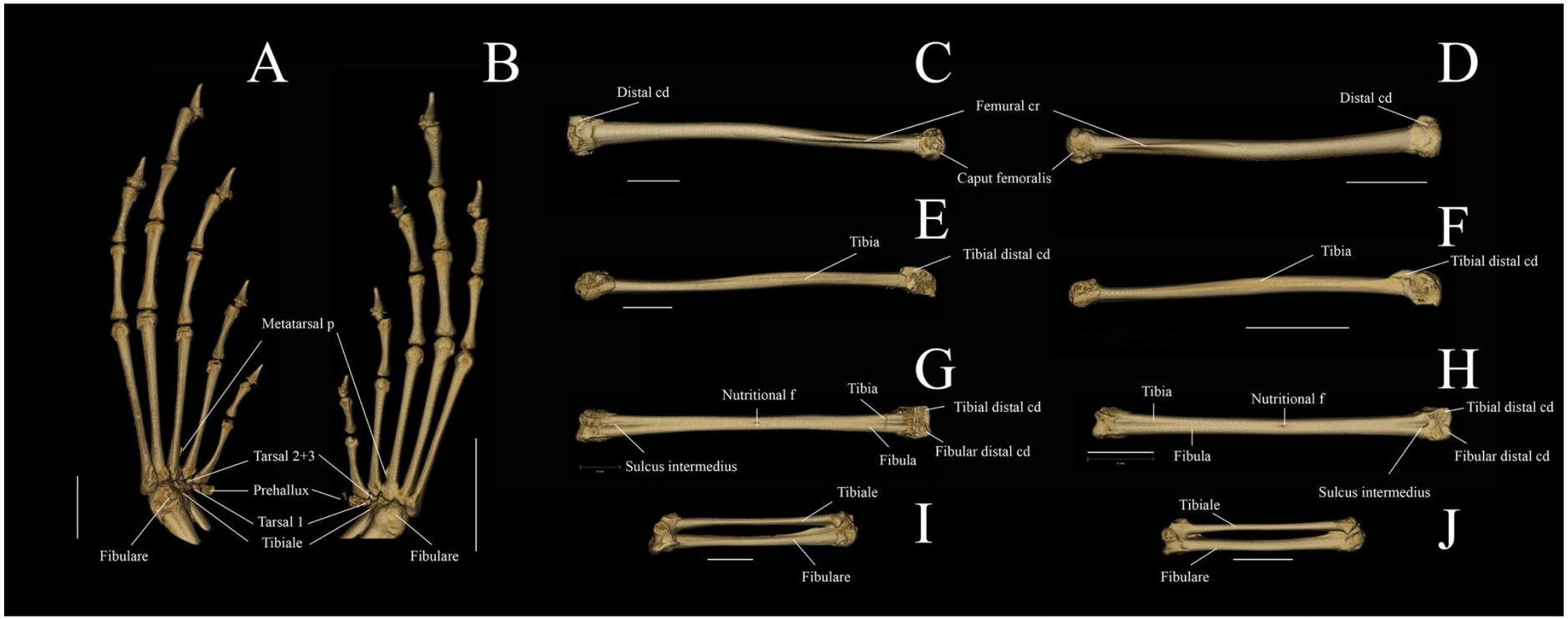

Figure 18. Calcified elements of the hindlimb skeleton of *Osteocephalus planiceps* MCP 14990 (A, C, E, G, I) and *O. vilarsi* INPAH 40470 (B, D, F, H, J). Scale bar = 5 mm.

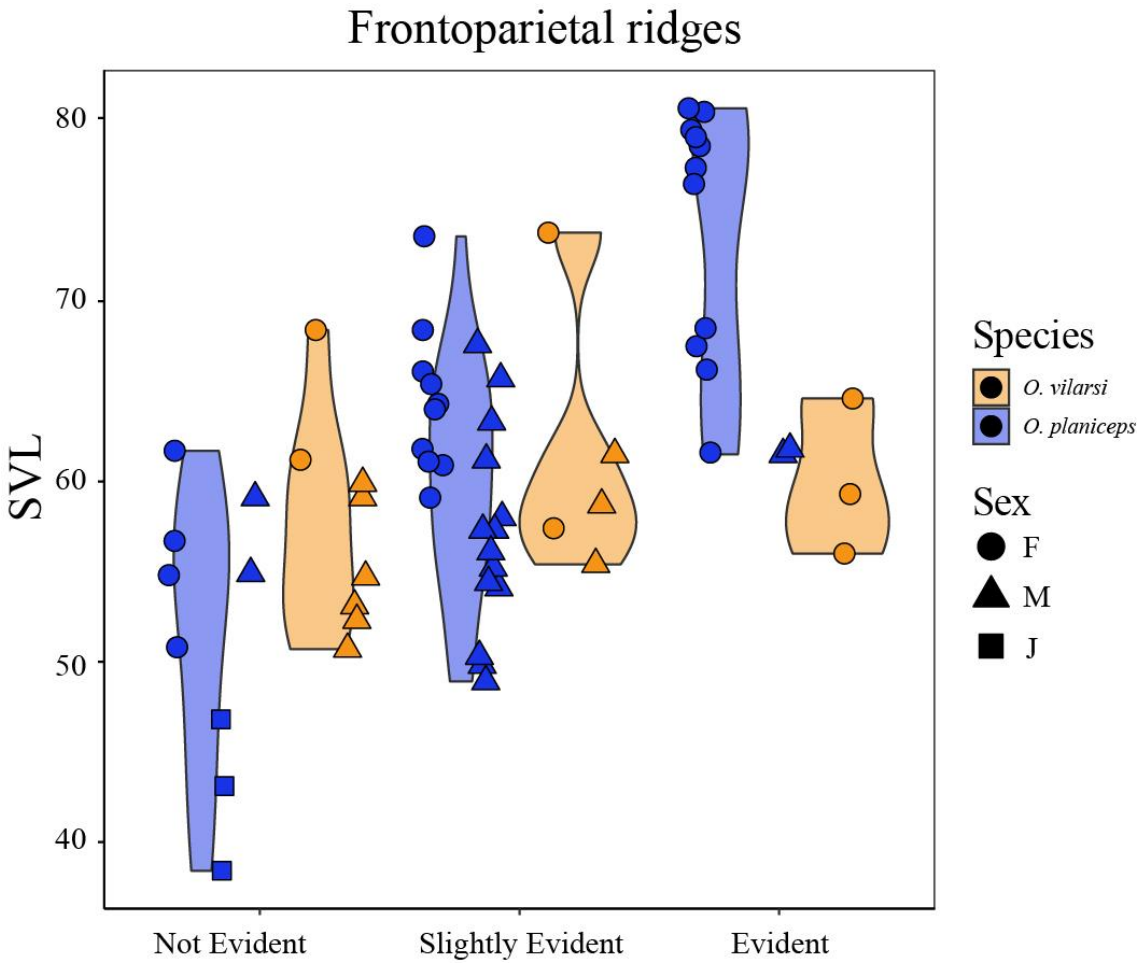

Figure 19. Variation of frontoparietal ridges in *Osteocephalus planiceps* and *O. vilarsi* according to ontogeny, sex, and size.

Pontifícia Universidade Católica do Rio Grande do Sul
Pró-Reitoria de Pesquisa e Pós-Graduação
Av. Ipiranga, 6681 – Prédio 1 – Térreo
Porto Alegre – RS – Brasil
Fone: (51) 3320-3513
E-mail: propesq@pucrs.br
Site: www.pucrs.br